Aplicaciones de Thermo-Calc y Dictra al diseño de aceros avanzados

Conexiones Thermo-Calc: Aplicaciones y Tutoriales

USACH

Felipe Castro Cerda
Associate Professor
Dept. of Metallurgy

Martes 15 de Octubre 2024

Acknowledgements

Usach-Dicyt – Research fundings
ANID – PhD Scholarship and Research projects
Dr A.K. Da Silva – Thermo-Calc AB
M.C. Ana Laura Hernandez – Thermo-Calc AB
Prof C. Goulas – UTwente
Prof R. Petrov – EEMMECS, UGent
Prof L. Kestens – EEMMECS, UGent
Dr T. Ros-Yañez – Cliffs Inc.
Dr E. Hernández – Cliffs Inc.

Background

USACH

Felipe Castro Cerda

- ✓ **Metallurgical Engineer, Msc in Materials Science – Usach, 2009**
- ✓ **Heat-Treatment Engineer – Equipos Mineros, 2009 – 2013**
- ✓ **PhD in Materials Science – USACH-UGent, 2013 – 2017**
- ✓ **Academic – USACH, 2017 – Present**

Research lines

- ✓ Steel processing
- ✓ Solid-solid phase transformations
- ✓ Recrystallization
- ✓ Characterization
- ✓ Computational thermodynamics

Ongoing projects

- ✓ Ultrafast heating of steel (Cliffs-Usach)
- ✓ Chemical patterning of steel (Fondecyt)
- ✓ Q&P for mining applications (Cliffs-Usach)
- ✓ Laser heat-treatments (UAlberta-Usach)

Outline

1. **Motivation**
2. **The third generation of advanced high strength steels**
3. **Formation of austenite**
   i. Massive mechanism
4. **Quench and partitioning**
   i. Constrained carbon equilibrium
   ii. Partitioning of carbon
5. **Summary**

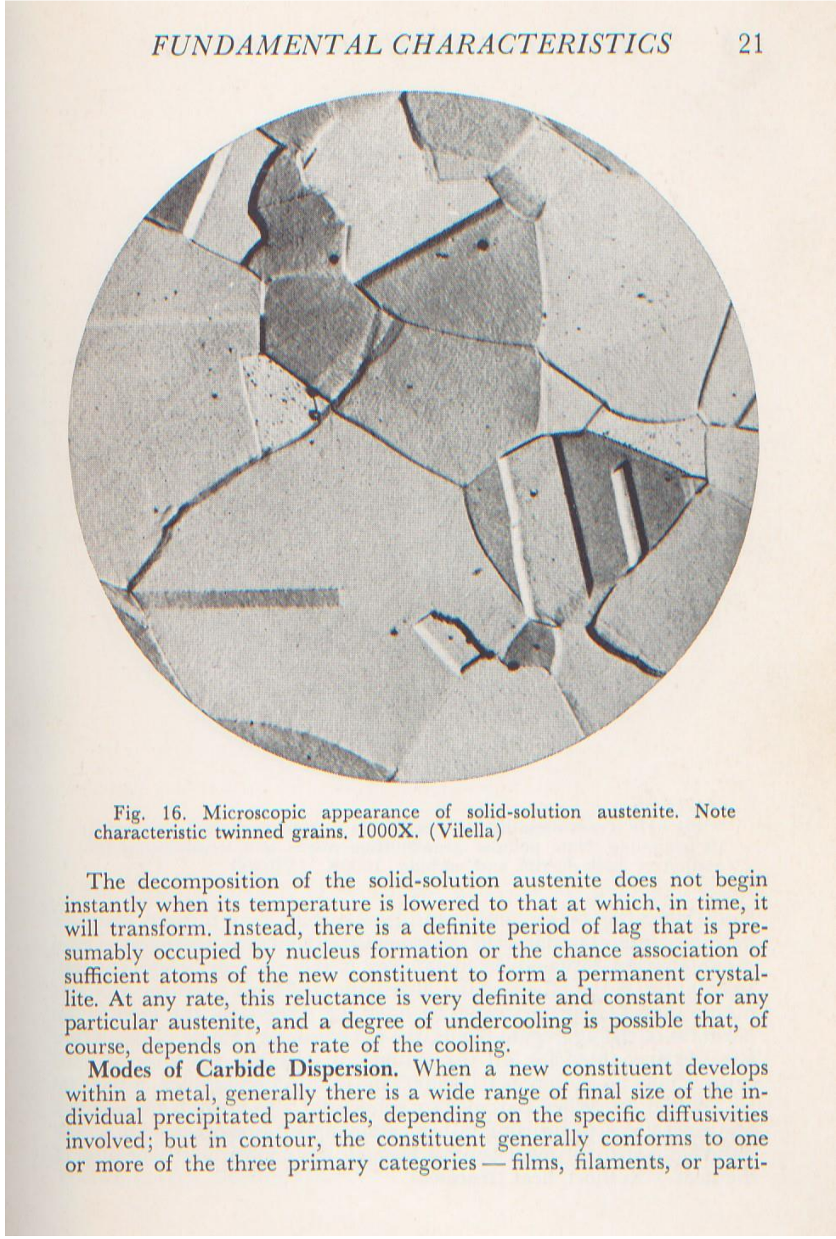

FUNDAMENTAL CHARACTERISTICS 21

Fig. 16. Microscopic appearance of solid-solution austenite. Note characteristic twinned grains. 1000X. (Vilella)

The decomposition of the solid-solution austenite does not begin instantly when its temperature is lowered to that at which, in time, it will transform. Instead, there is a definite period of lag that is presumably occupied by nucleus formation or the chance association of sufficient atoms of the new constituent to form a permanent crystallite. At any rate, this reluctance is very definite and constant for any particular austenite, and a degree of undercooling is possible that, of course, depends on the rate of the cooling.

Modes of Carbide Dispersion. When a new constituent develops within a metal, generally there is a wide range of final size of the individual precipitated particles, depending on the specific diffusivities involved; but in contour, the constituent generally conforms to one or more of the three primary categories — films, filaments, or parti-

EC Bain and HW Paxton, *"Alloying elements in steel"* 2nd ed., ASM Int. Metals Park, OH,

Motivation

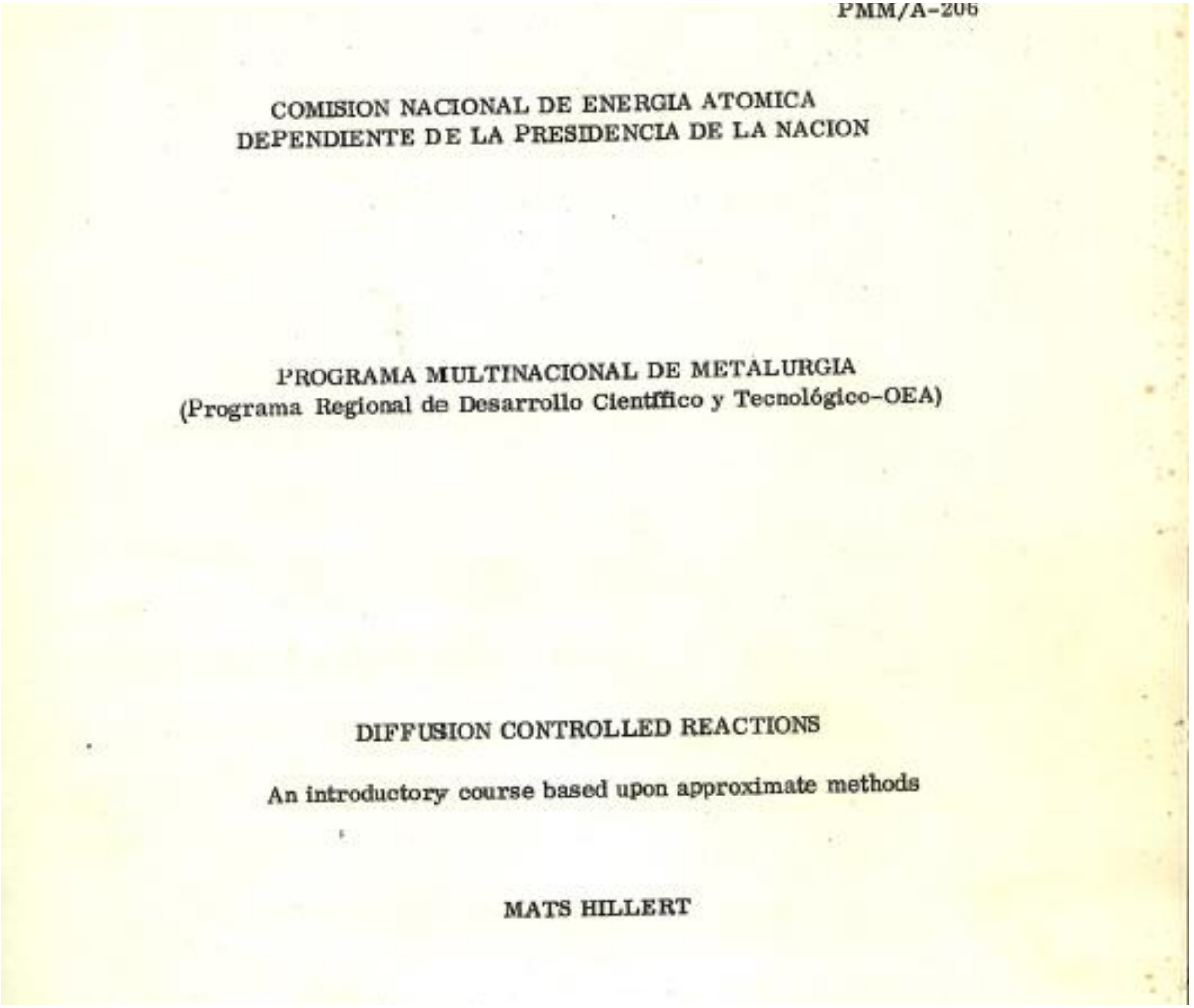

PMM/A-206

COMISION NACIONAL DE ENERGIA ATOMICA
DEPENDIENTE DE LA PRESIDENCIA DE LA NACION

PROGRAMA MULTINACIONAL DE METALURGIA
(Programa Regional de Desarrollo Científico y Tecnológico-OEA)

DIFFUSION CONTROLLED REACTIONS

An introductory course based upon approximate methods

MATS HILLERT

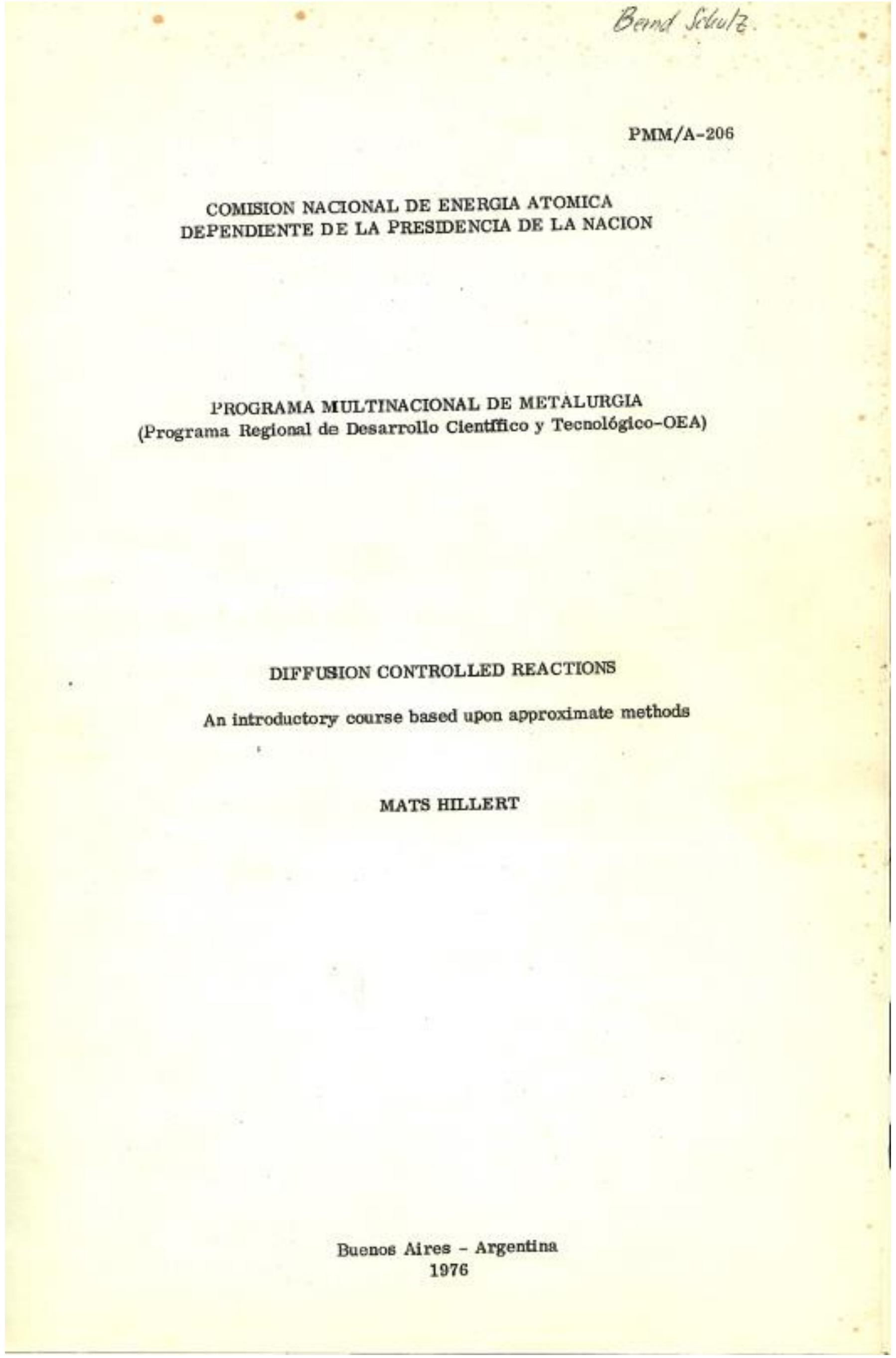

Bernd Schulz

PMM/A-206

COMISION NACIONAL DE ENERGIA ATOMICA
DEPENDIENTE DE LA PRESIDENCIA DE LA NACION

PROGRAMA MULTINACIONAL DE METALURGIA
(Programa Regional de Desarrollo Científico y Tecnológico-OEA)

DIFFUSION CONTROLLED REACTIONS

An introductory course based upon approximate methods

MATS HILLERT

Buenos Aires - Argentina
1976

Motivation

CONTENT

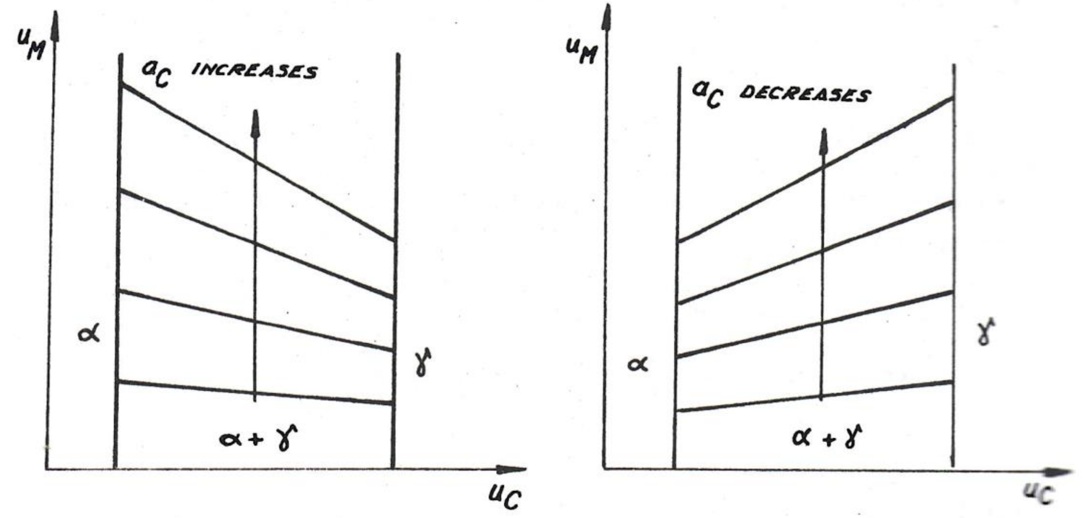

It should be noticed that this calculation is independent upon the actual slope of the phase boundaries and of the isoactivity lines for carbon in α and γ. However there is a mutual dependence of the slopes of tie-lines, phase boundaries and isoactivity lines, which is demonstrated in the next two diagrams.

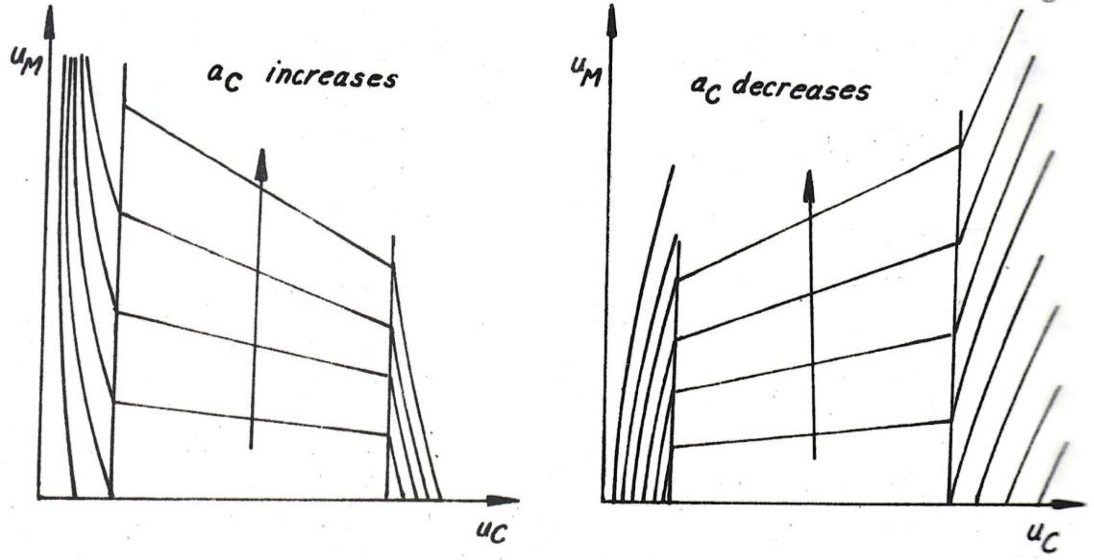

Motivation

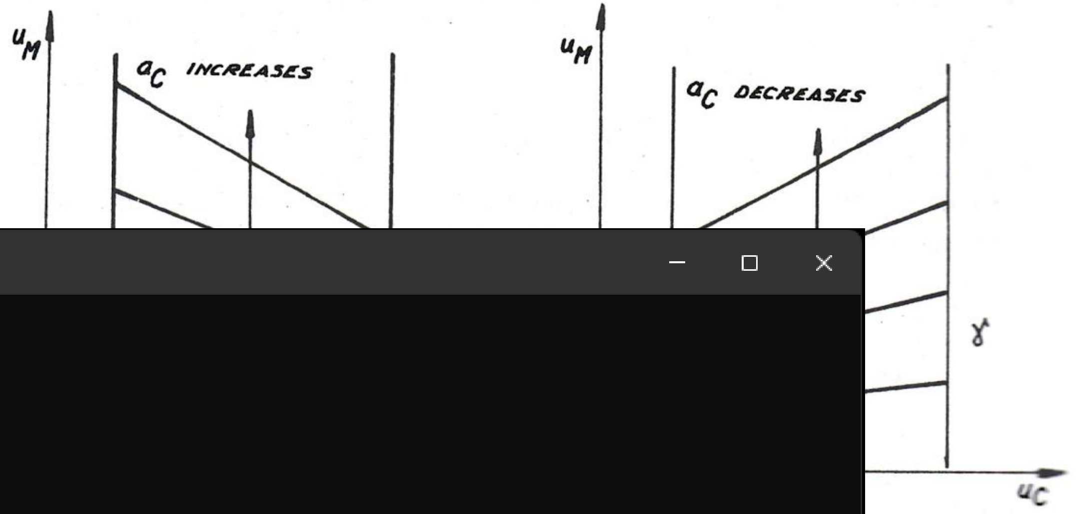

CO

A. DIF
1. I
2. I
3. I
4. V

B. MA
5. S
6. C
7. I
8. T
9. T
10. T
11. T

C. DIF
12. S
13. T
14. T
15. I

D. TRA
16. I
17. T
18. F
19. I
20. I
21. T
22. Deviation from local equilibrium

E. PROBLEMS

C:\Users\Asus\AppData\Local

```
Open Calphad (OC) software version   6.056 , linked 2022-07-16
with command line monitor version 71

This program is available with a GNU General Public License.
either version 2 of the License, or any later version.
It includes the General Thermodynamic Package, version GTP-3.30,
Hillert's equilibrium calculation algorithm version HMS-3.0 ,
step/map/plot software version SMP-2.30 using GNUPLOT 5.2 graphics.
Numerical routines are extracted from LAPACK and BLAS and
the assessment procedure uses LMDIF from ANL.

Linked with OpenMp for parallel execution
 Warning, no environment variable OCHOME but local help file
 Working directory is: C:\Users\Asus\AppData\Local\Programs\OpenCalphad\OC6
--->OC6:
```

pon the actual
arbon in α and
ie-lines, phase
next two diagrams.

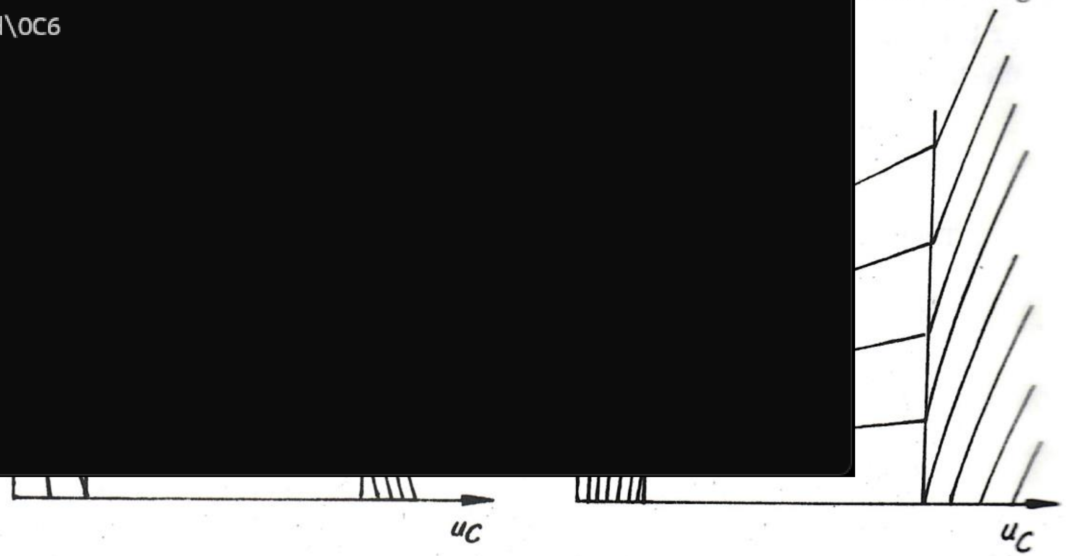

Third generation advanced high strength steels

AHSS – Designed for automotive industry demands

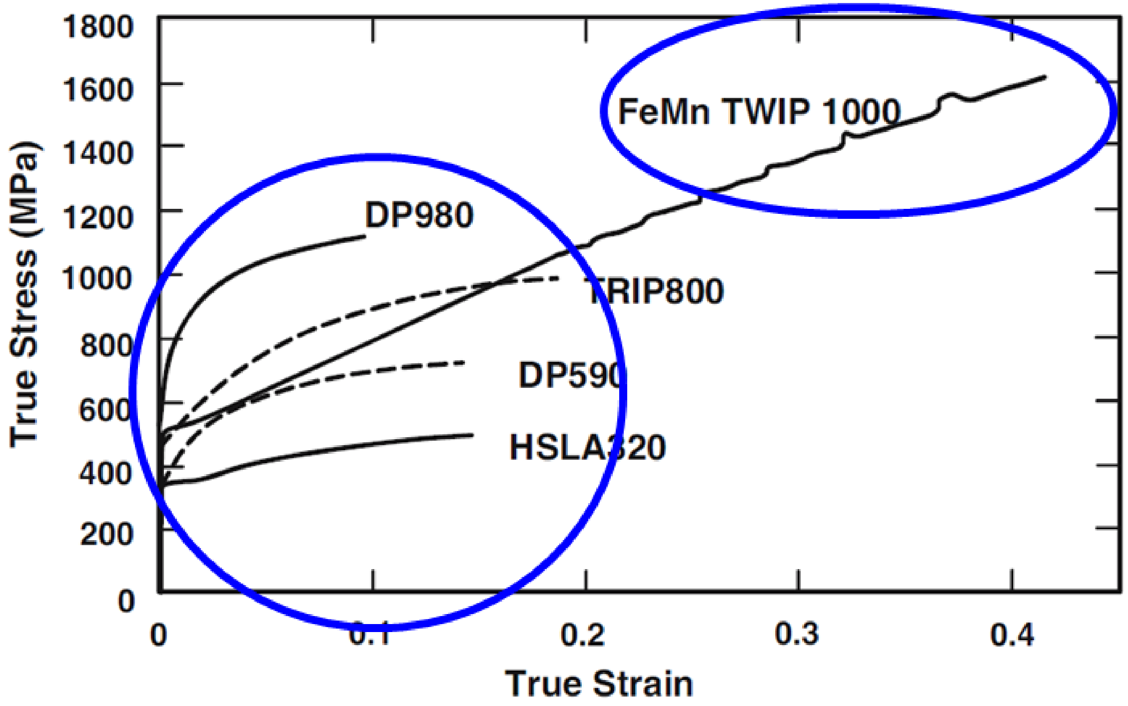

2nd Generation AHSS

High amount of alloying elements

1st Generation AHSS

Good strength/formability, but not sufficient

Source: D. K. Matlock and J. G. Speer, Third Generation of AHSS: Microstructure Design Concepts, in A. Haldar, D. Bhattacharjee, and S. Suwas (Eds) Proc. of the Int. Conference on Microstructure and Texture in Steels and Other Materials, Jamshedpur, India, 2008.

Third generation advanced high strength steels

AHSS – Designed for automotive industry demands

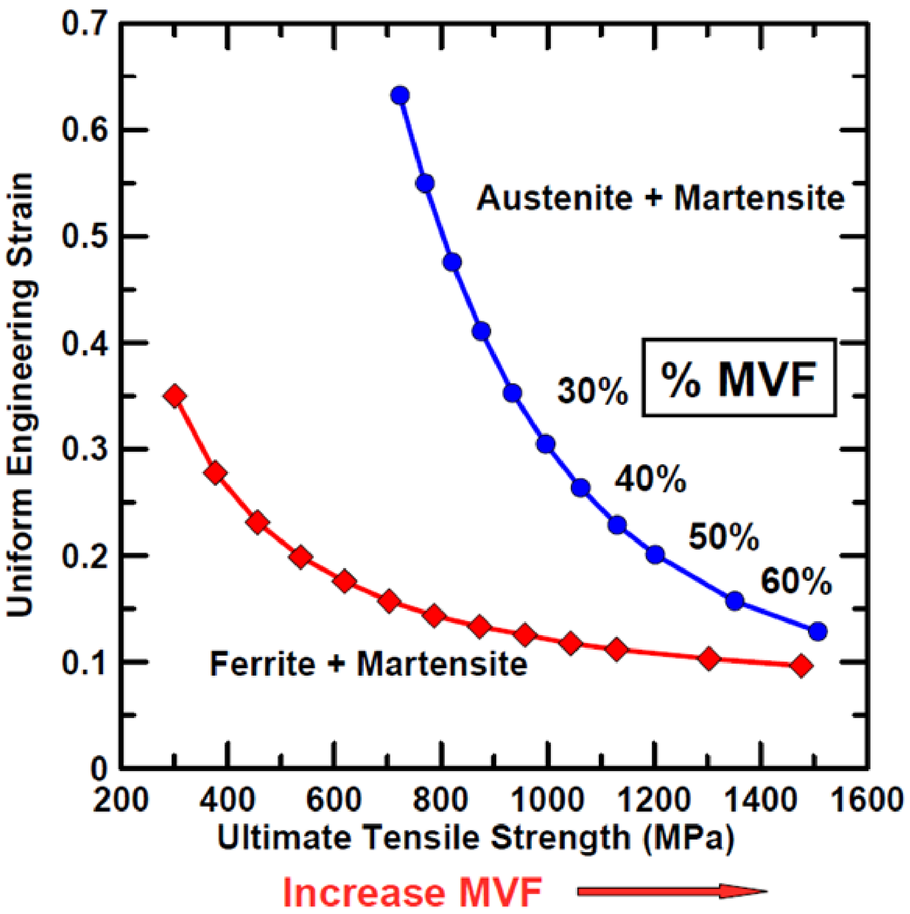

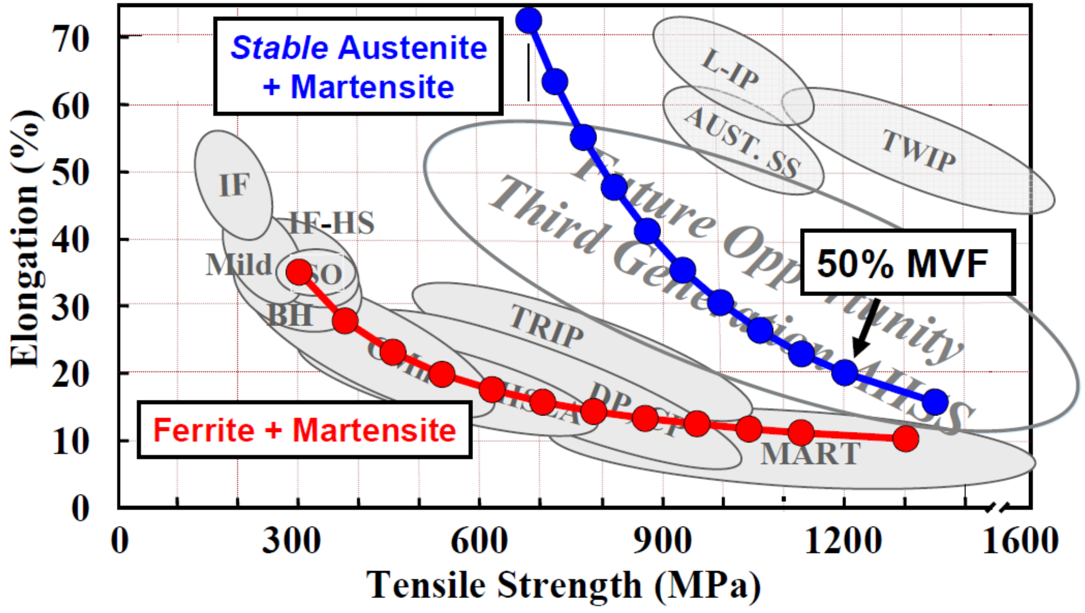

Q&P, Medium Mn steels

Third Generation AHSS are *not achievable* by enhanced DP steels!!!

D.K. Matlock and J.G. Speer,, Proc. of the 3rd Int. Conf. on Structural Steels, ed. by H.C. Lee, The Korean Inst. of Metals and Materials, Seoul, Korea, 2006, pp. 774-781.

Third generation advanced high strength steels

Combined strengthening effects:

Ultrafast heating of cold-rolled steel

- ✓ Grain refinement
- ✓ Multiphase structure
- ✓ Partially recrystallized
- ✓ Compositional heterogeneities
- ~~✓ *Heavy alloying strategy*~~

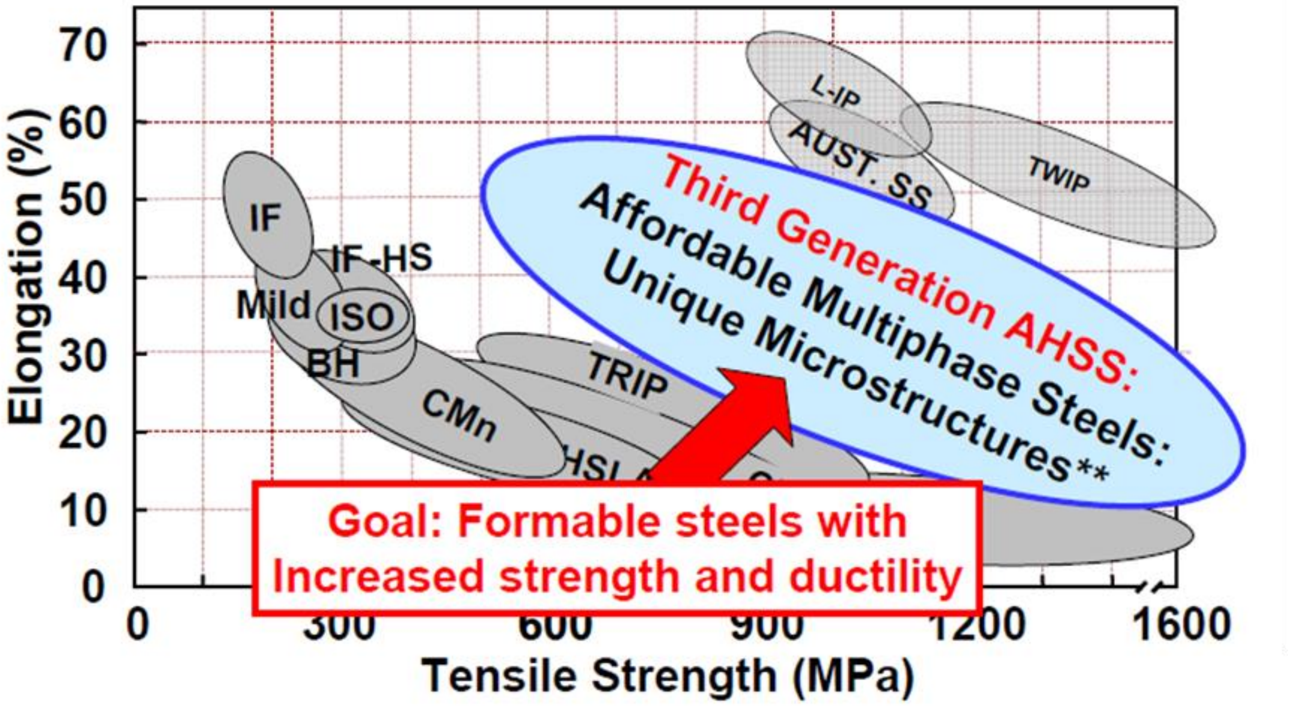

Wide range of microstructures and mechanical properties

Third generation advanced..

Combined strengthening effects:

Ultrafast heating of cold-rolled steel

- ✓ **Grain refinement**
- ✓ **Multiphase structure**
- ✓ **Partially recrystallized**
- ✓ **Compositional heterogeneities**
- ✓ ~~***Heavy alloying strategy***~~

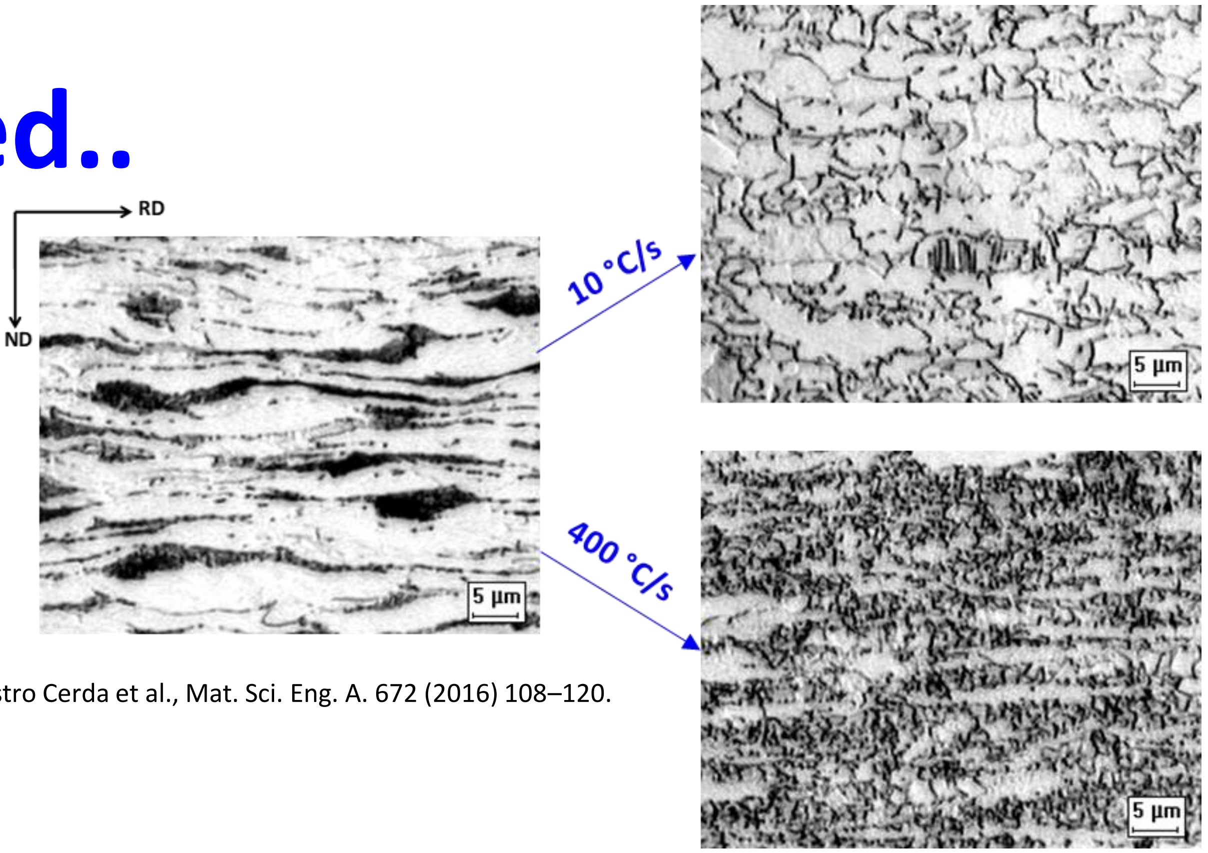

F.M. Castro Cerda et al., Mat. Sci. Eng. A. 672 (2016) 108–120.

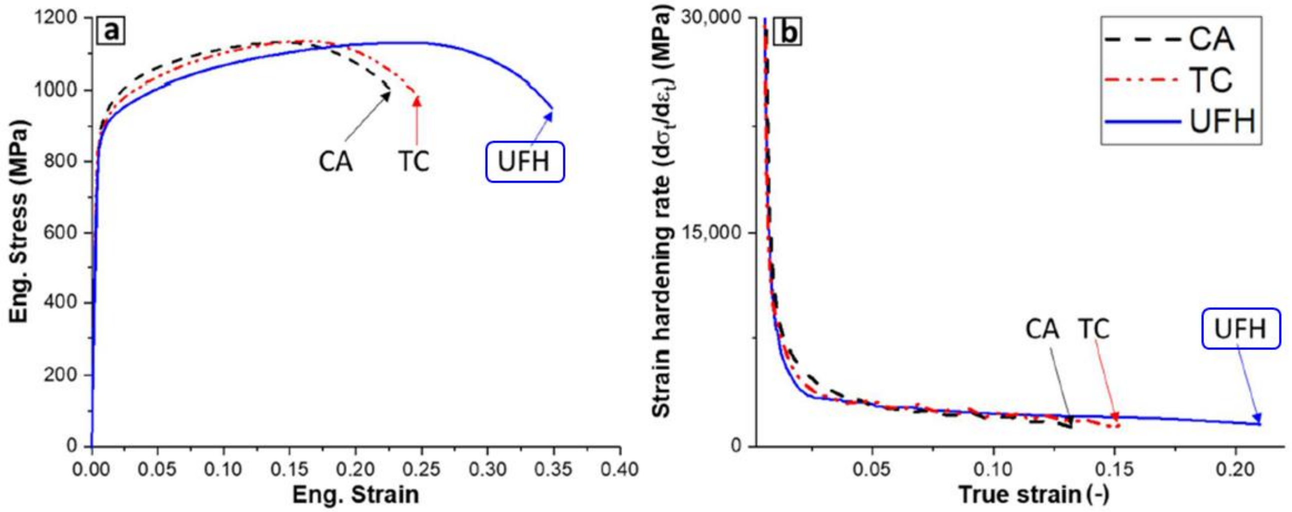

E. Hernandez-Duran, et al., *Metals* **2021**, *11*, 1041.

Austenite formation

Milestones

- ✓ Bain, 1939
- ✓ Mehl, 1943
- ✓ Gridnev & Trefilov, 1954
- ✓ Haworth & Parr, 1965
- ✓ Paxton, 1967
- ✓ Judd & Paxton, 1968
- ✓ Speich et al., 1969
- ✓ Hillert et al., 1971

0.1 wt. % C steel, >500 °C/s

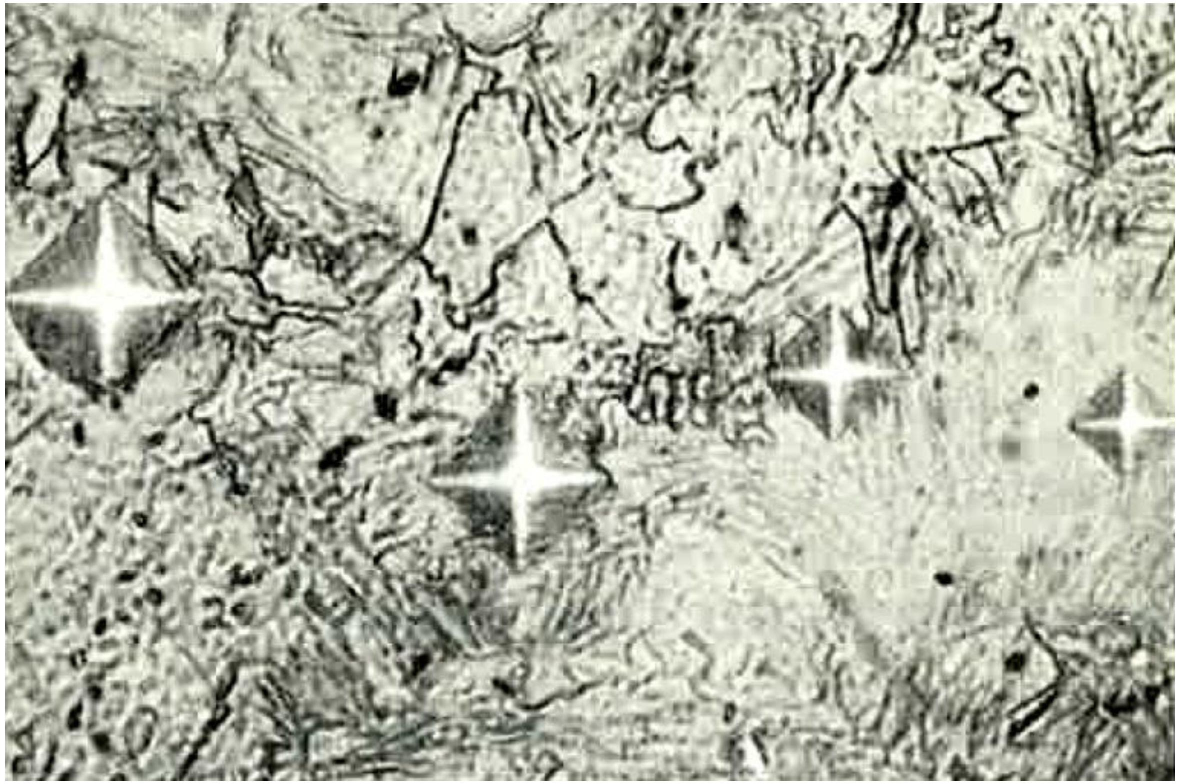

K. J. Albut & S. Garber, Effect of heating rate on the elevation of the critical temperatures of low-carbon mild steel, J. Iron and Steel Inst., 204, 1217 (1966).

Austenite formation

Isothermal growth of austenite

$$v = \frac{D_C^{\alpha} \Delta u_C^{\alpha} + D_C^{\gamma} \Delta u_C^{\gamma}}{S(u_C^{\gamma/\alpha} - u_C^{\alpha})}$$

(towards pearlite)

M. Hillert, K. Nilsson, L..E. Torndahl, *Effect of alloying elements on the formation of austenite and dissolution of cementite,* J. Iron Steel Inst. 49–66 (1971).

$$v^{\gamma\to\alpha} = \frac{D_C^{\gamma}\left(X_C^{\gamma} - X_C^{\gamma/\alpha}\right)}{L\left(X_C^{\gamma/\alpha} - X_C^{\alpha/\gamma}\right)}$$

(towards ferrite)

H.B. Aaron, D. Fainstein, G.R. Kotler, J. Appl. Phys. 41 (1970) 4404–4410.

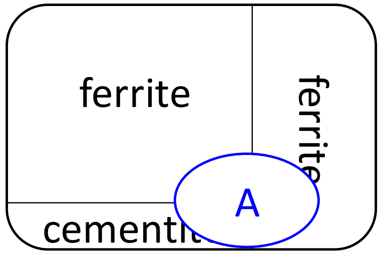

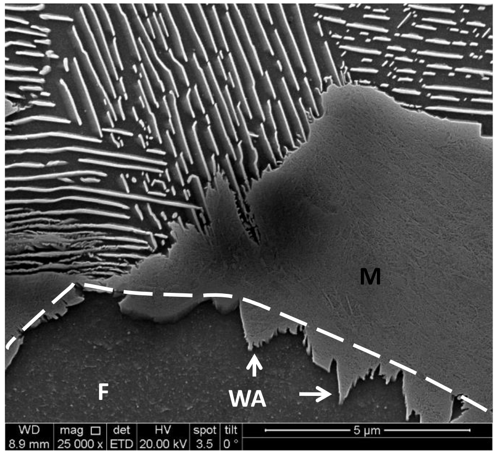

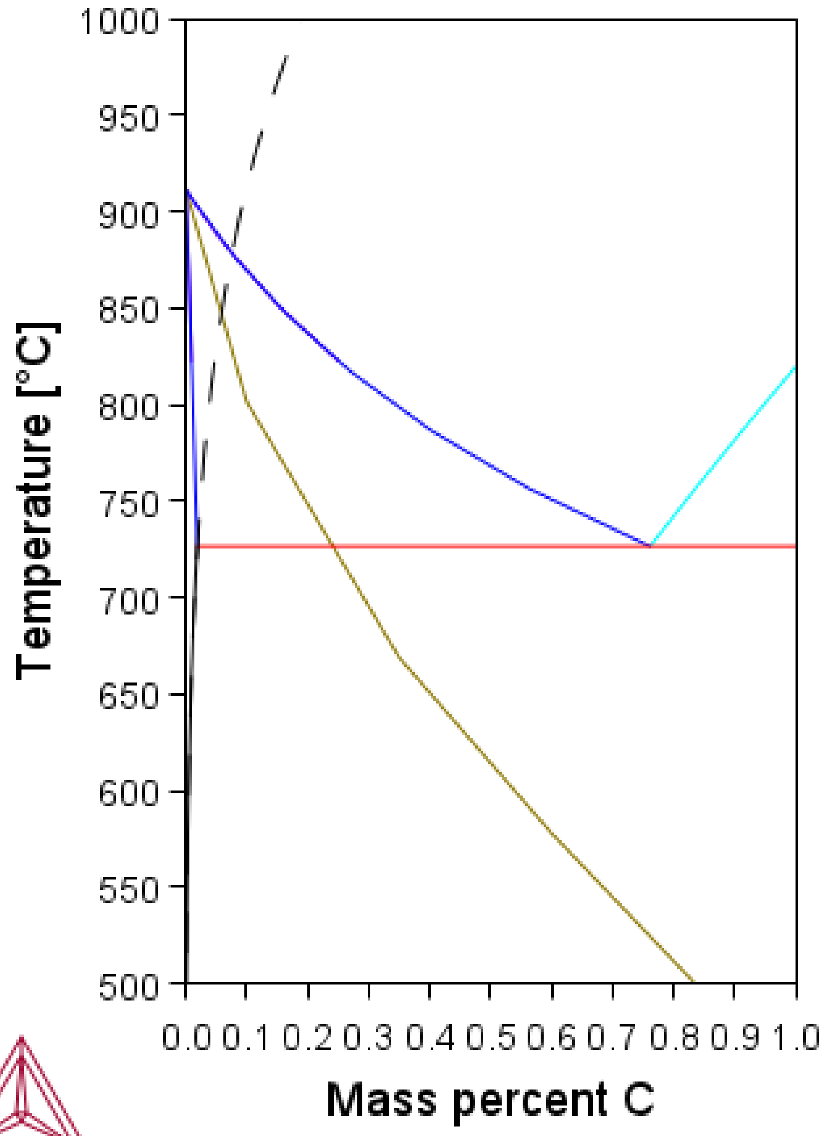

Austenite formation

Continuous growth of austenite

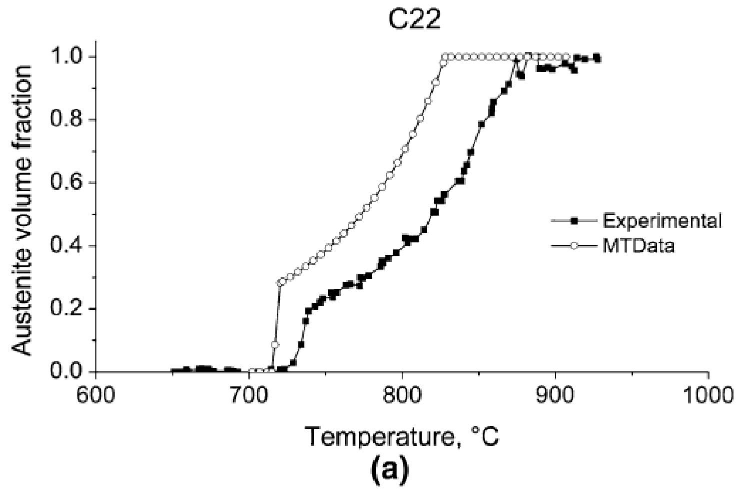

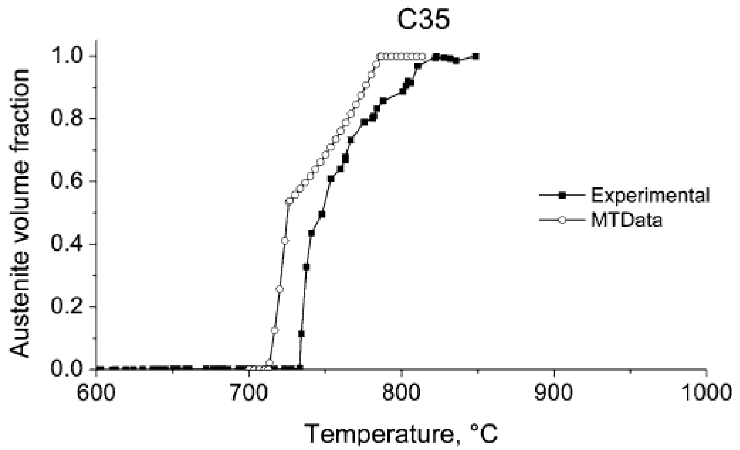

VI Savran et al. *Metall Mater Trans A* **41**, 583–591 (2010)

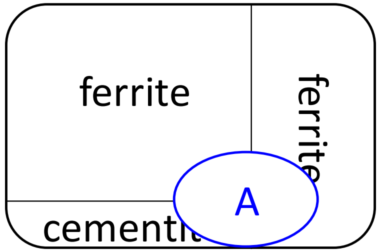

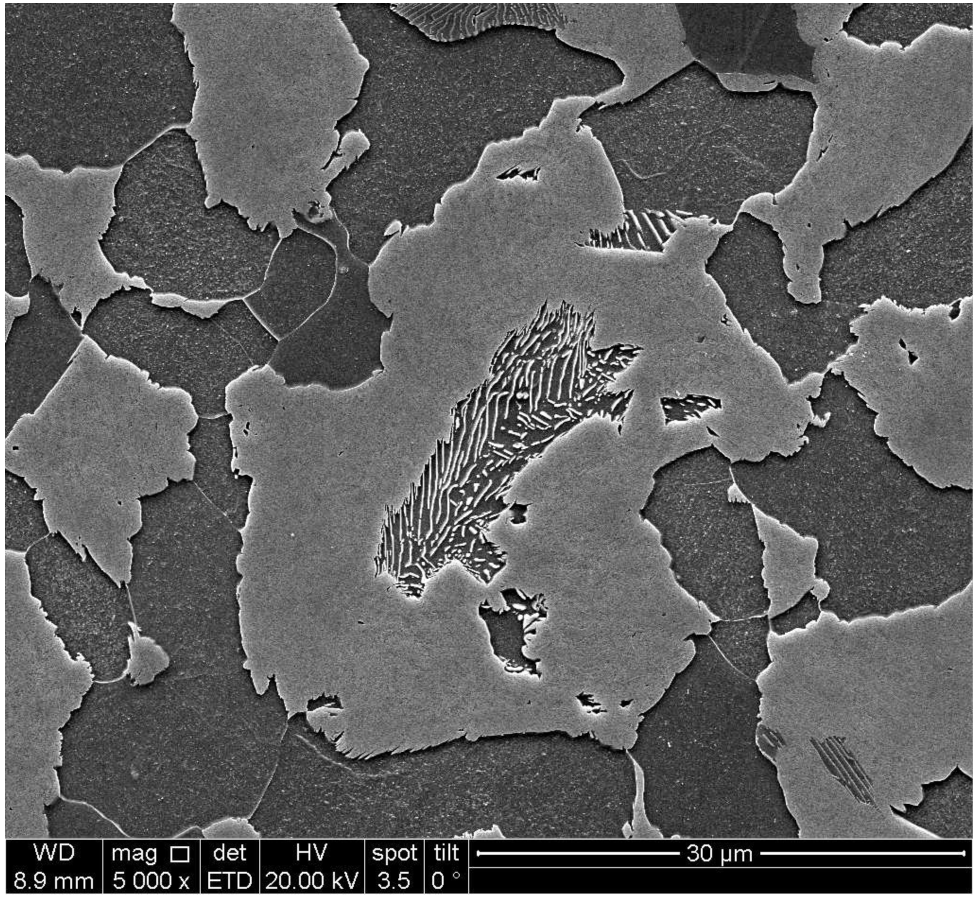

F.M. Castro Cerda et al,. Mater. Des. 116 (2017) 448–460

The temperature variation of the phase fraction shows the fast growth towards pearlite first, then the growth towards ferrite, yet both are occurring at the same time.

Austenite formation

Rapid heating conditions

Same stages as the slow continuous growth of austenite

Curves are displaced to the right; the transformation occurs faster (increase of $v^{\gamma\to\alpha}$)

The kinetic change is more significant in the growth of austenite towards proeutectoid ferrite.

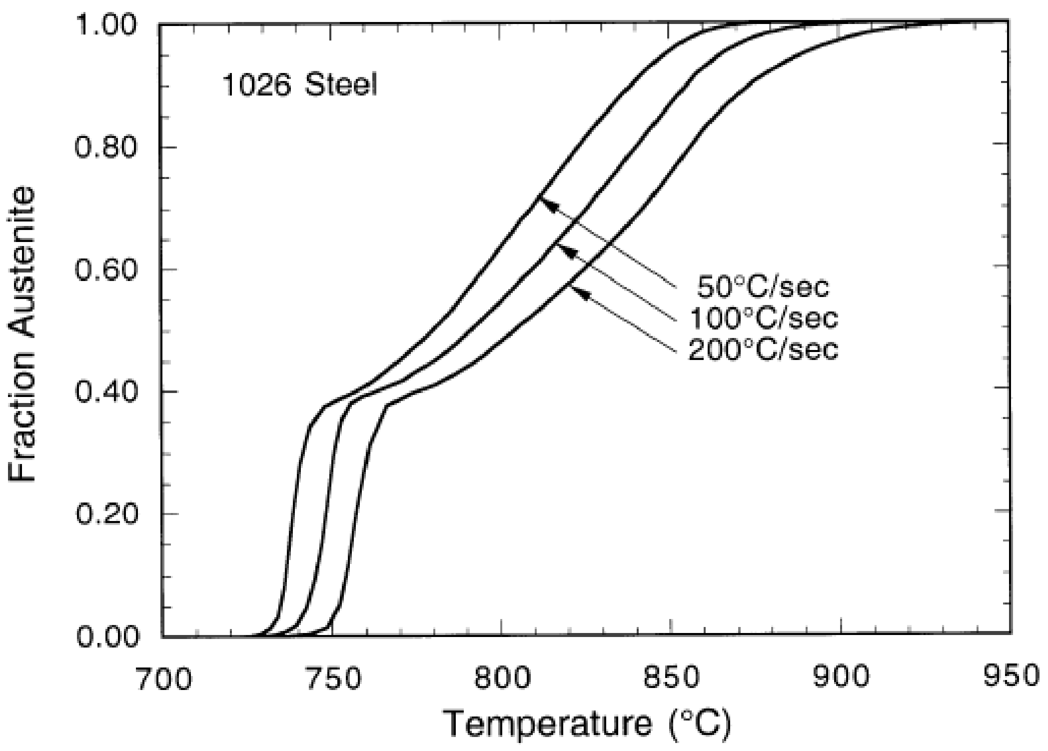

RC Dykhuizen et al. *Metall Mater Trans B* **30**, 107–117 (1999)

$$v^{\gamma\to\alpha} = \frac{D_C^{\gamma}\left(X_C^{\gamma} - X_C^{\gamma/\alpha}\right)}{L\left(X_C^{\gamma/\alpha} - X_C^{\alpha/\gamma}\right)}$$

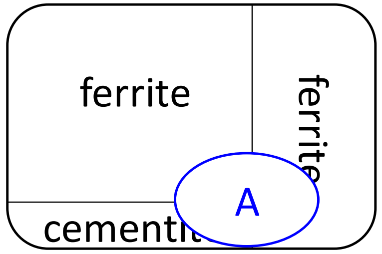

Austenite formation

Growth of austenite into ferrite 0,2 %C

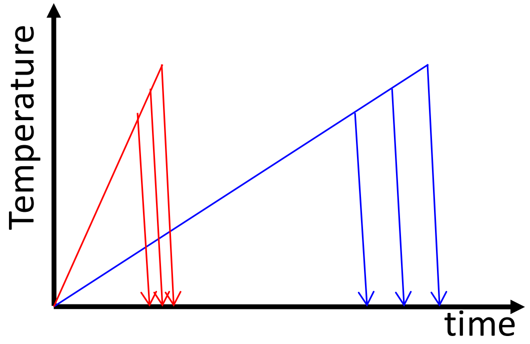

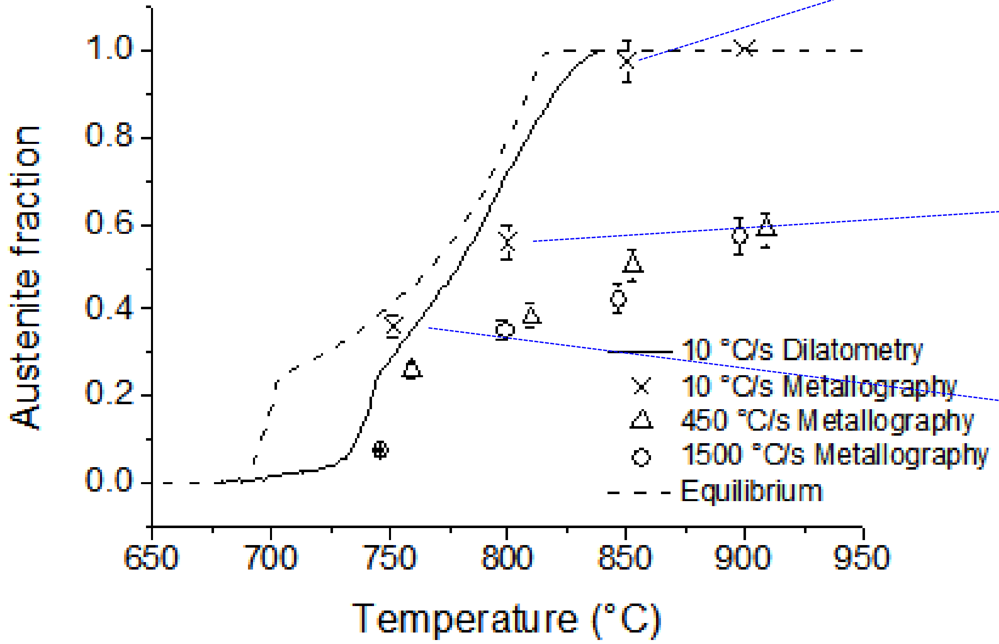

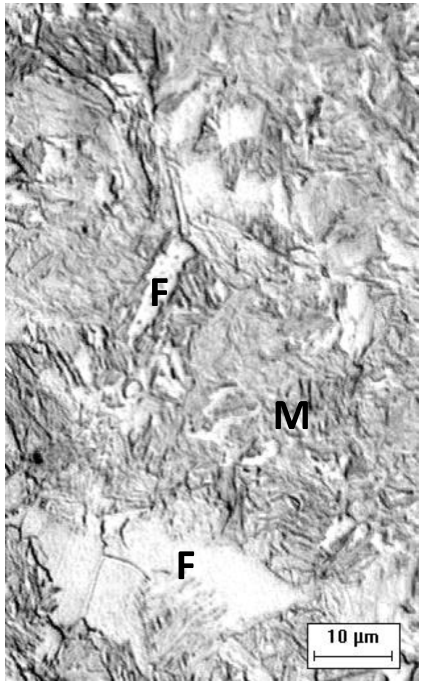

T_P = 851 °C

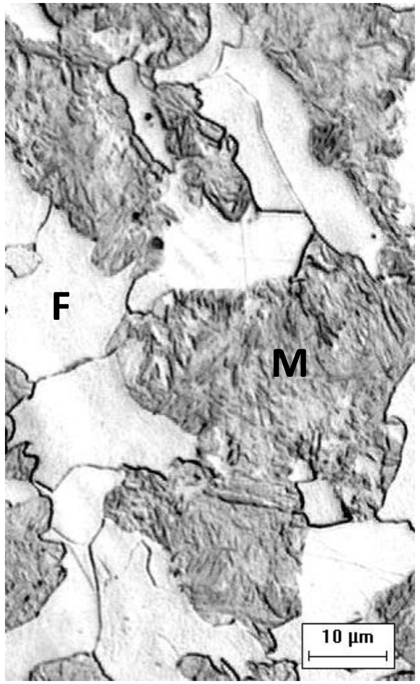

T_P = 800 °C

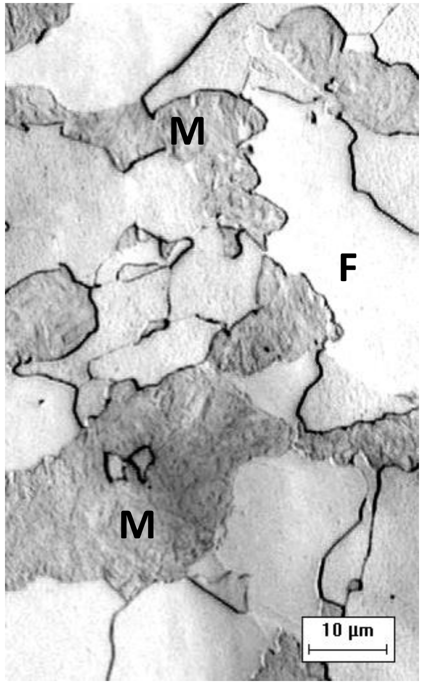

T_P = 760 °C

F.M. Castro Cerda et al. Mater. Des. 116 (2017) 448–460

Austenite formation

Growth of austenite into ferrite 0,2 %C

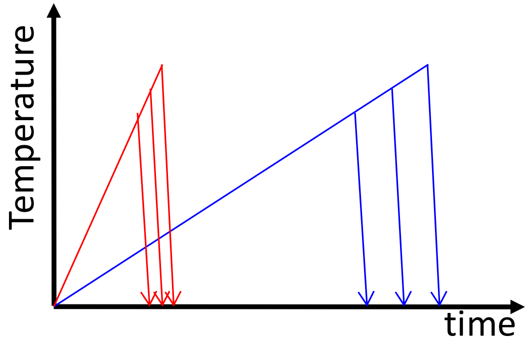

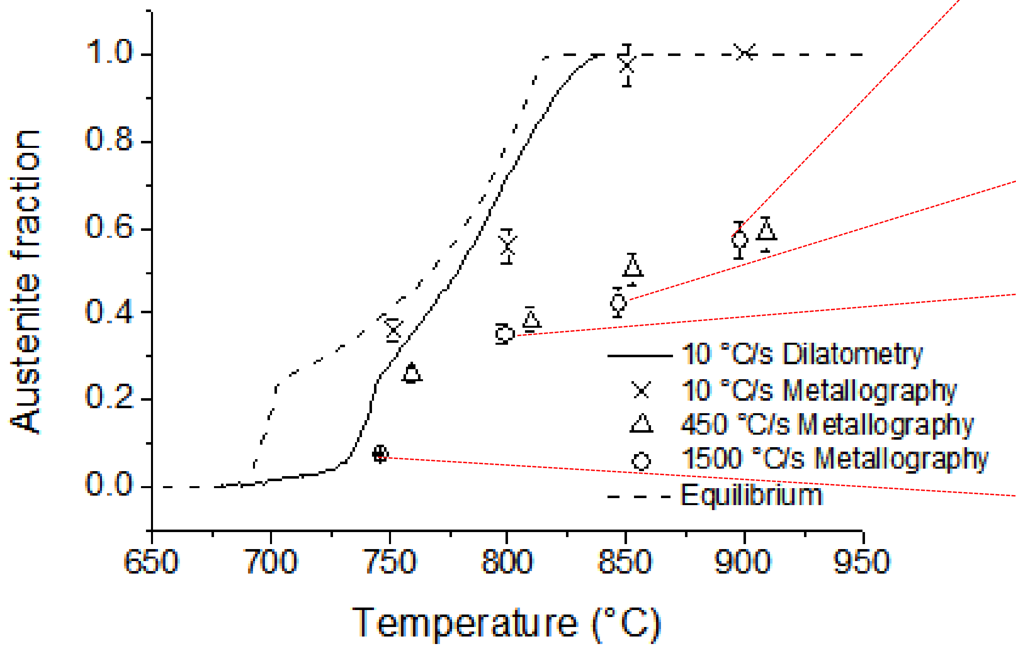

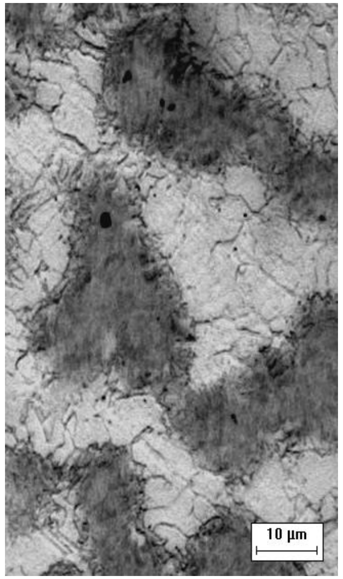

T_P = 898 °C

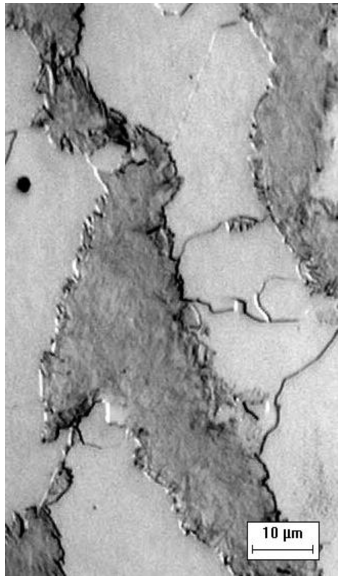

T_P = 847 °C

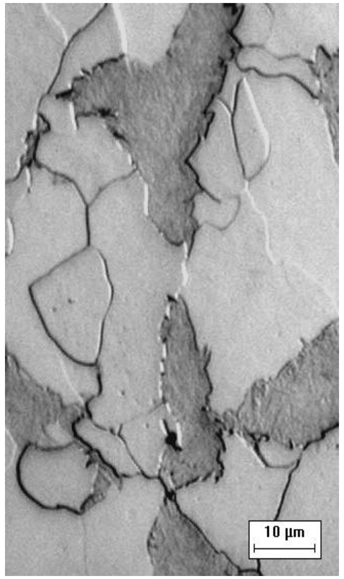

T_P = 746 °C

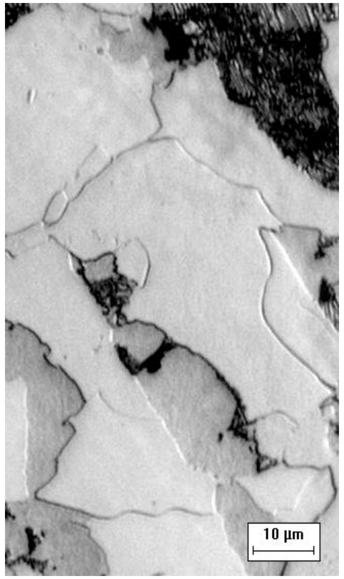

T_P = 799 °C

F.M. Castro Cerda et al. Mater. Des. 116 (2017) 448–460

Austenite formation

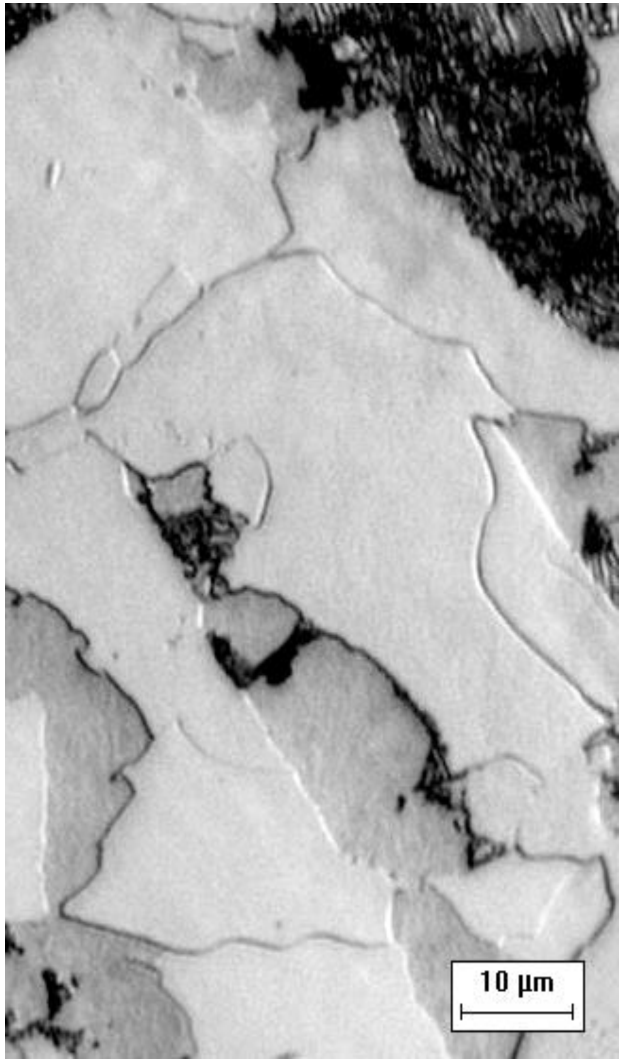

T_P = 746 °C

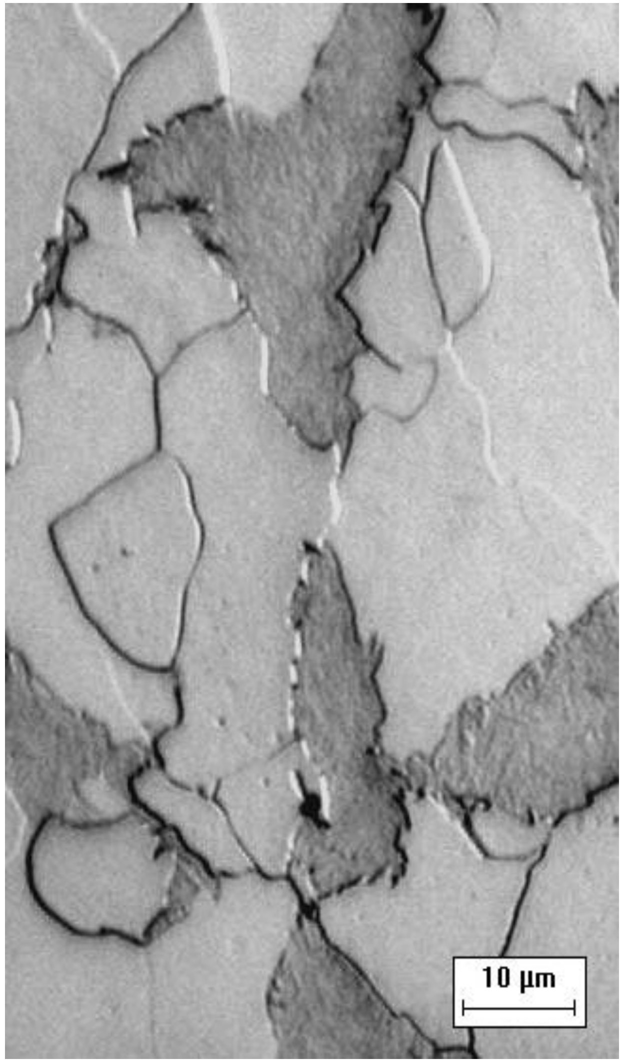

T_P = 799 °C

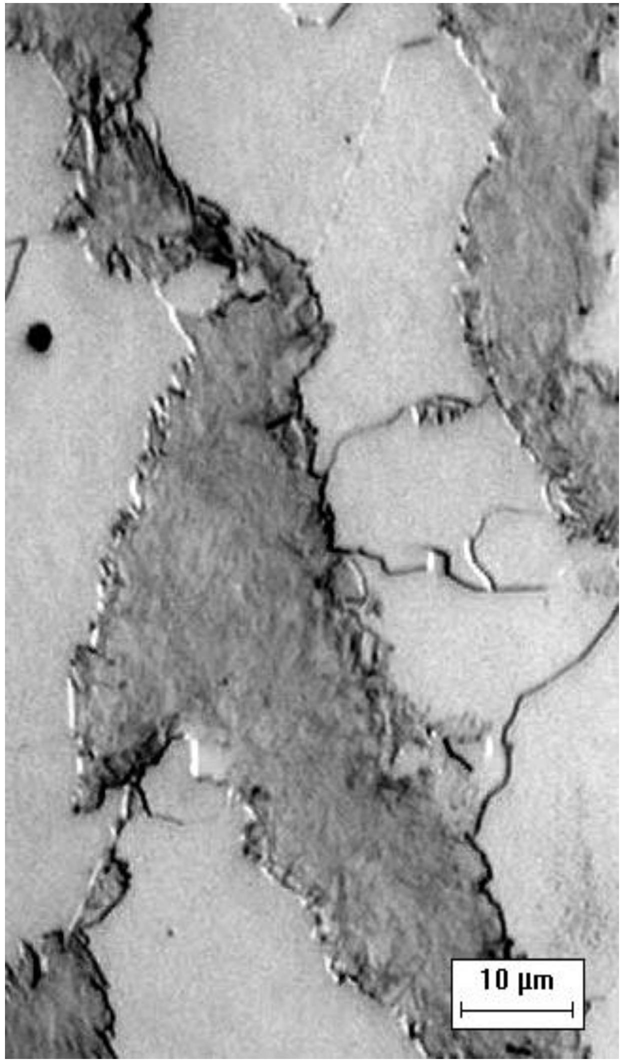

T_P = 847 °C

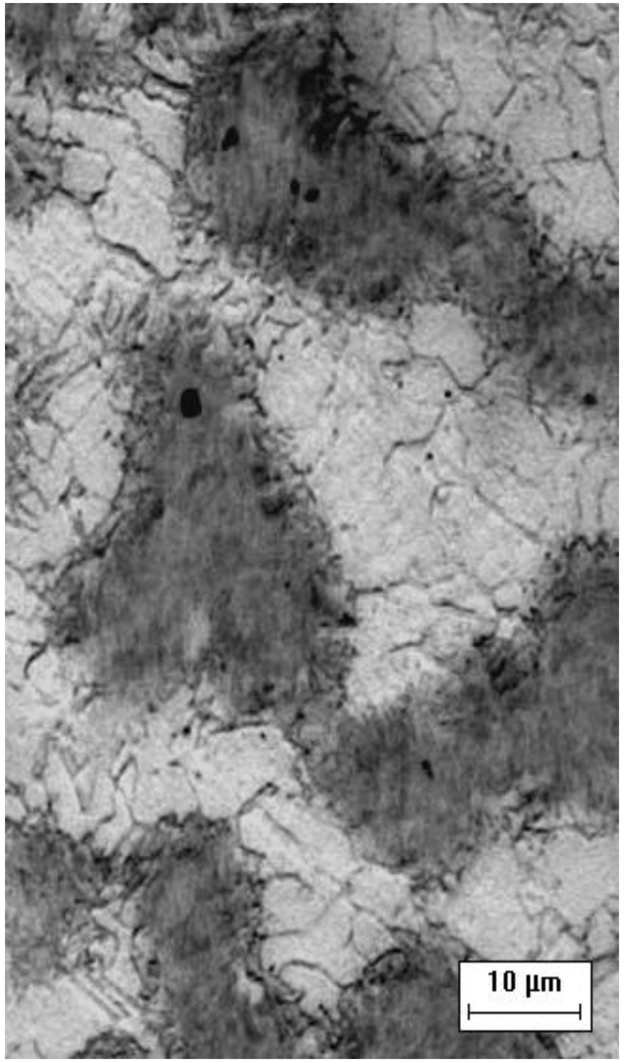

T_P = 898 °C

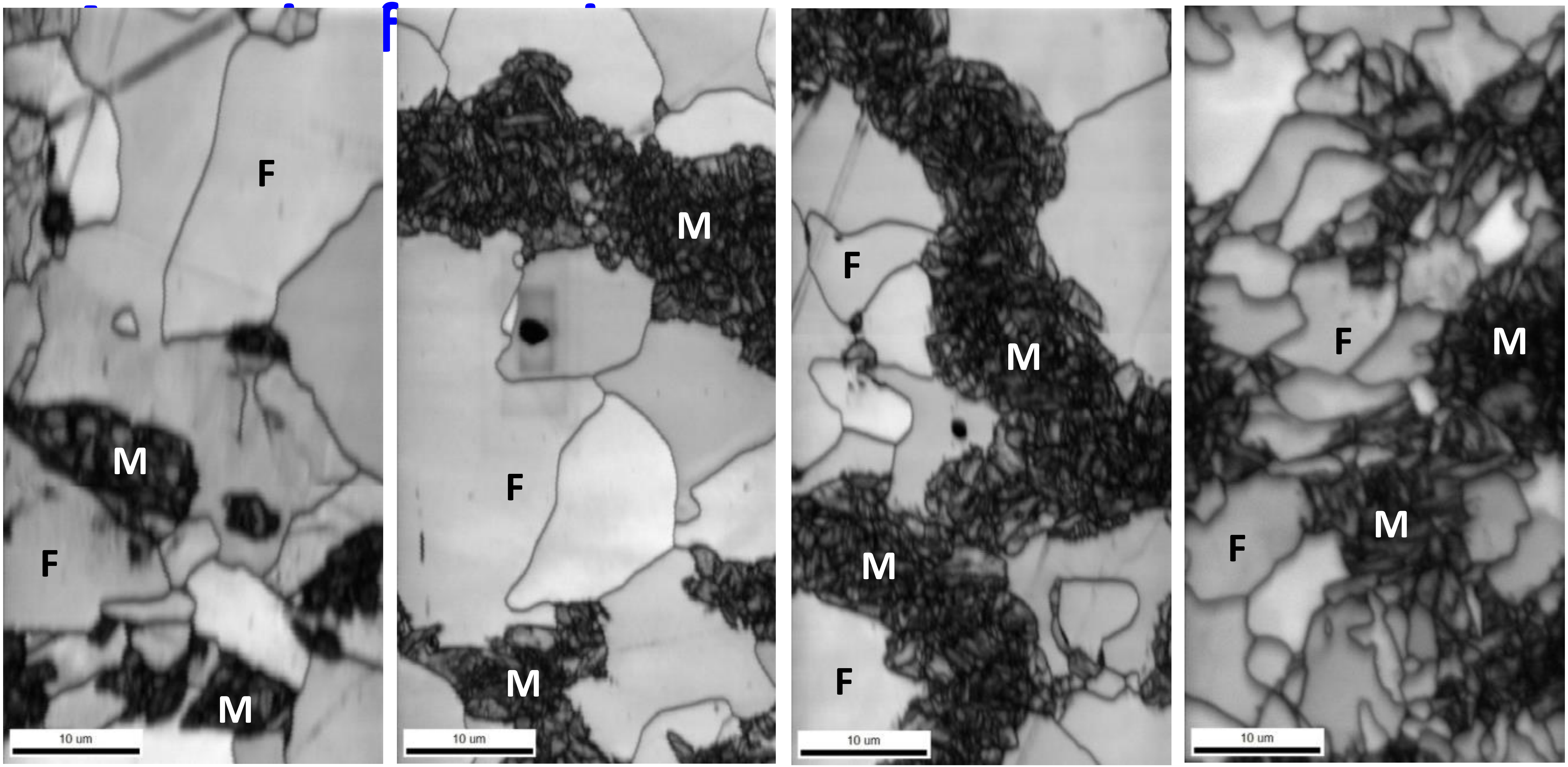

T_P = 746 °C T_P = 799 °C T_P = 847 °C T_P = 898 °C

Austenite formation

Rapid heating conditions

Growth of austenite into ferrite **0,2 %C**

$(Fe,C)^{\alpha} + Fe_3C \rightarrow (Fe,C)^{\gamma}$

$\Delta G^{\alpha+\theta \rightarrow \gamma} = G^{\gamma} - (G^{\alpha} + G^{\theta})$

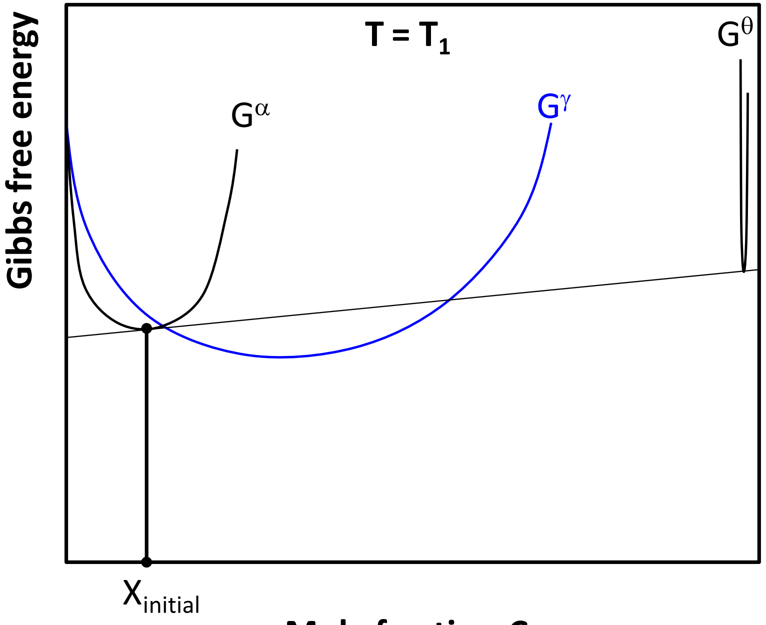

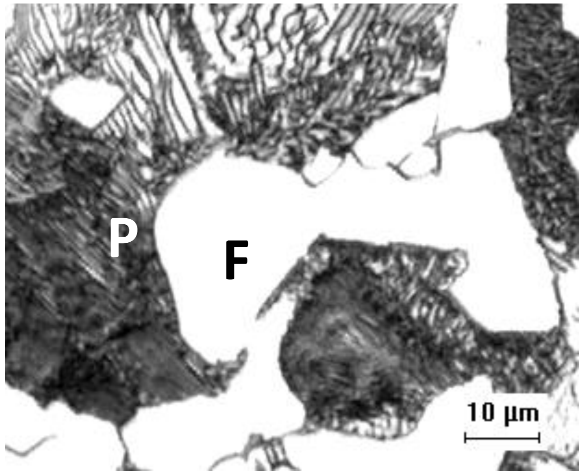

Initial (average) composition is **meaningless**

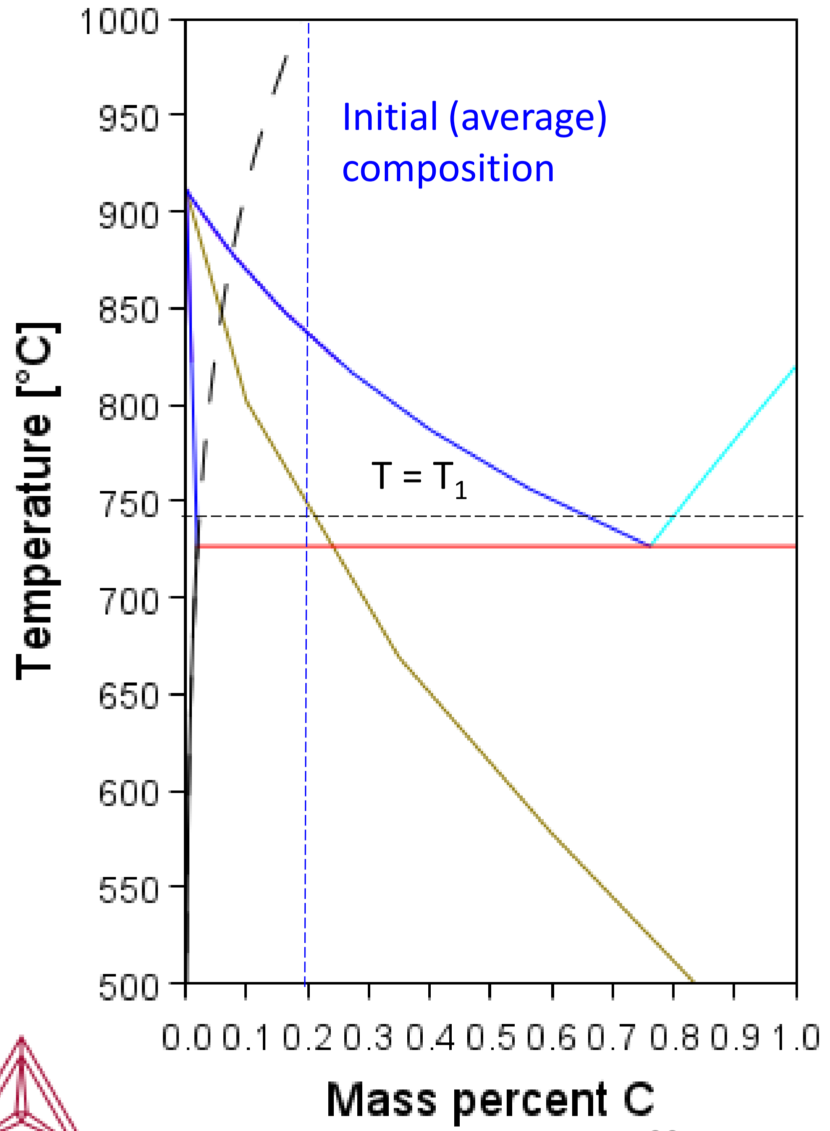

Austenite formation

Rapid heating conditions

Growth of austenite into ferrite 0,2 %C

$(Fe,C)^{\alpha} + Fe_3C \rightarrow (Fe,C)^{\gamma}$

$\Delta G^{\alpha+\theta\rightarrow\gamma} = G^{\gamma} - (G^{\alpha})$

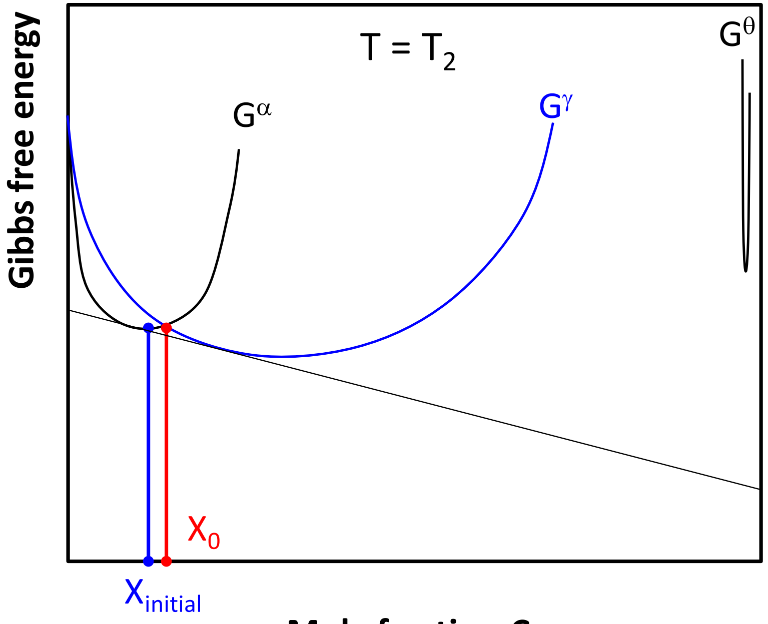

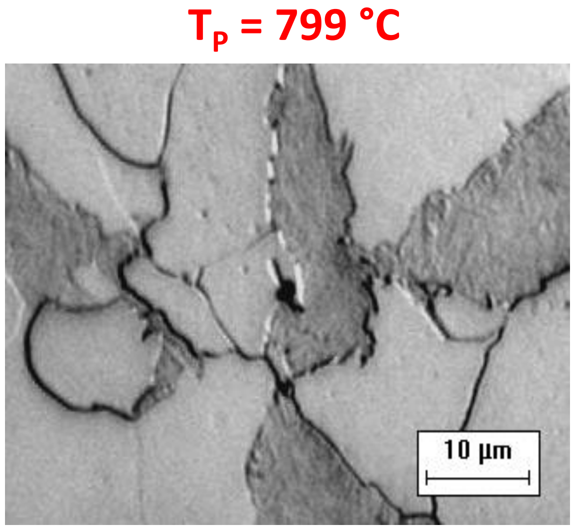

Initial (average) composition is meaningless

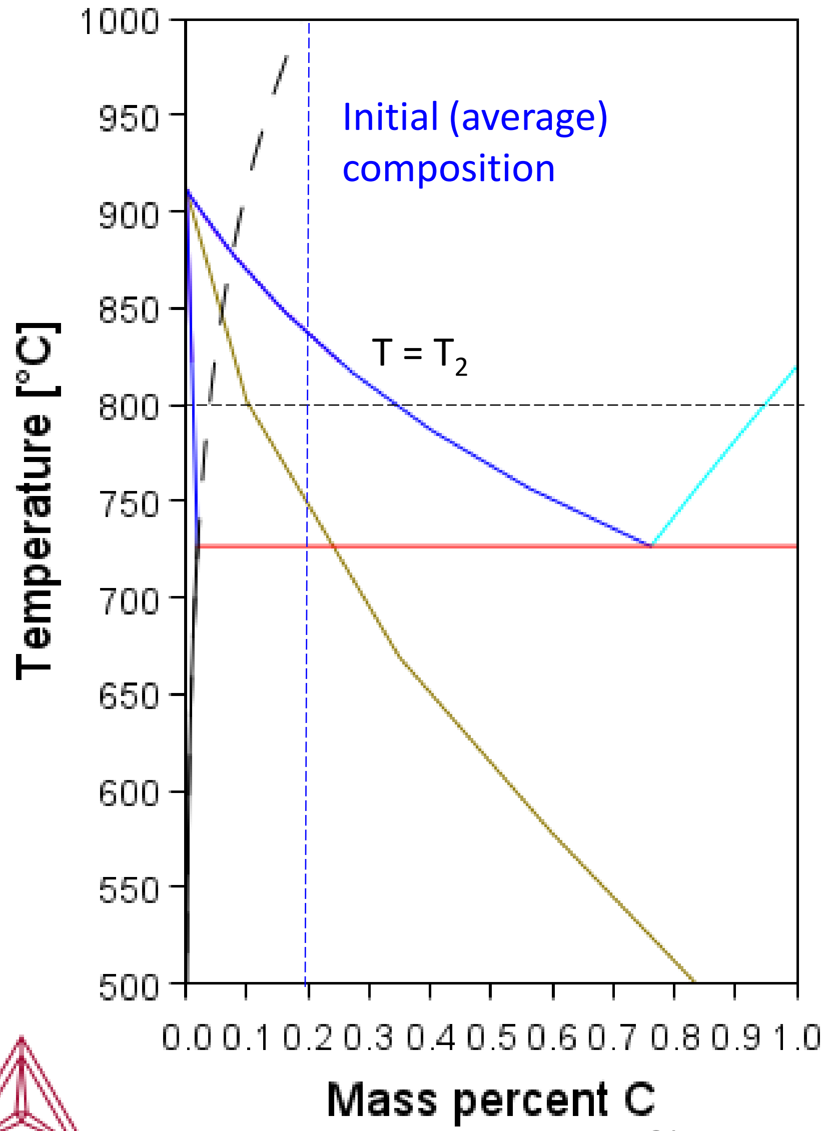

Austenite formation

Rapid heating conditions

Growth of austenite into ferrite **0,2 %C**

$(Fe,C)^{\alpha} + Fe_3C \rightarrow (Fe,C)^{\gamma}$

$\Delta G^{\alpha+\theta\rightarrow\gamma} = G^{\gamma} - (G^{\alpha})$

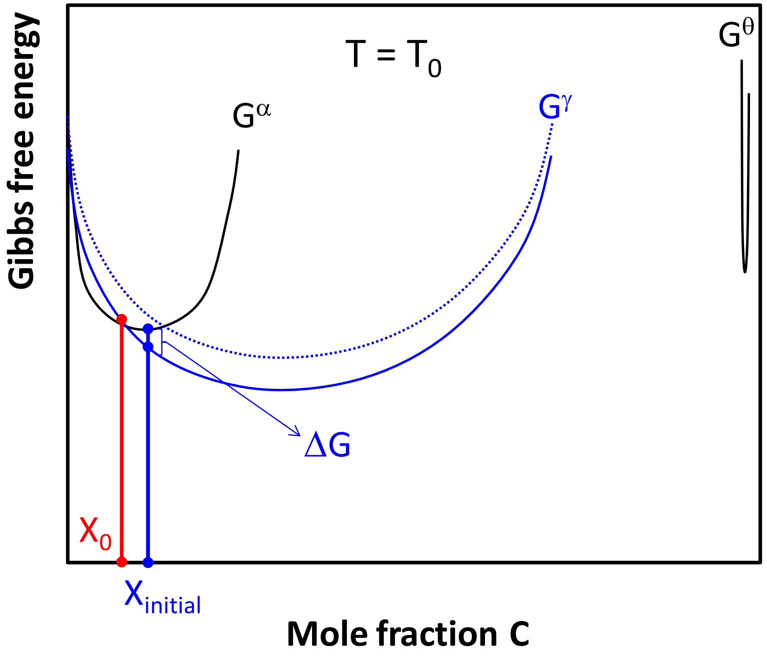

T_P = 847 °C

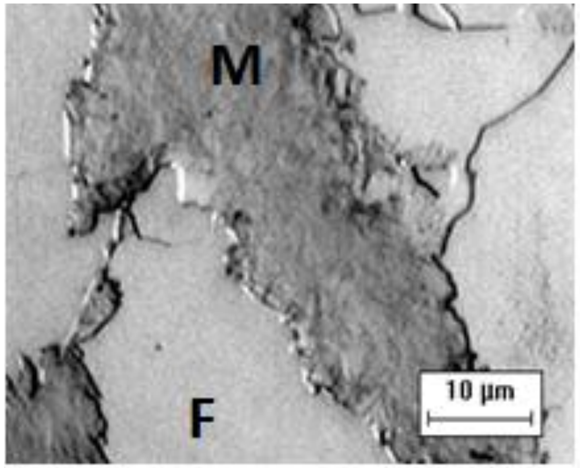

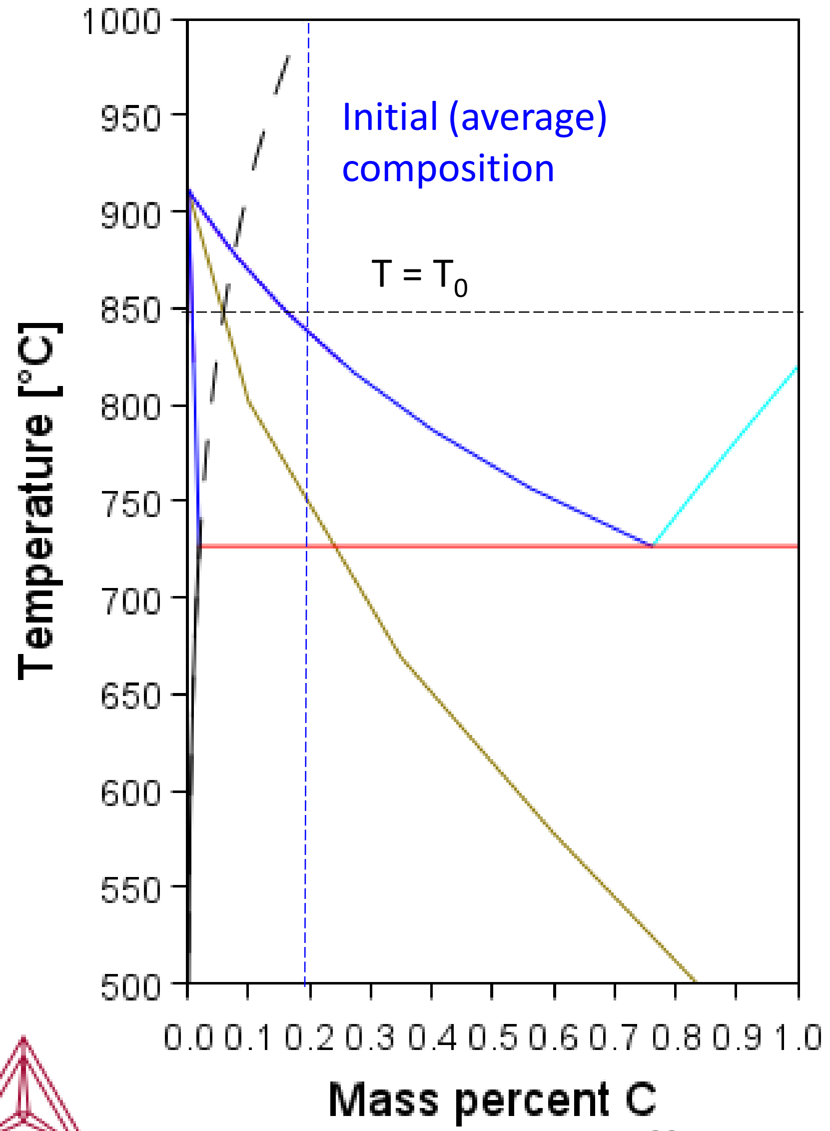

Austenite formation

VIII. CONCLUSIONS

From the above considerations it appears natural to expect all the massive transformations in binary alloys and the alloy invariant reactions in Fe-M-C alloys to obey the line starting at the solvus point rather than the line starting at the T_0 point. Of course, the exact nature of the local equilibrium at any combination of temperature and interface velocity depends upon the properties of the interface. This is something we can only speculate about at present. One can construct models and simulate the reaction on a computer. As an

Hillert, M., *Metall Mater Trans A* **15A**, 411–419 (1984)

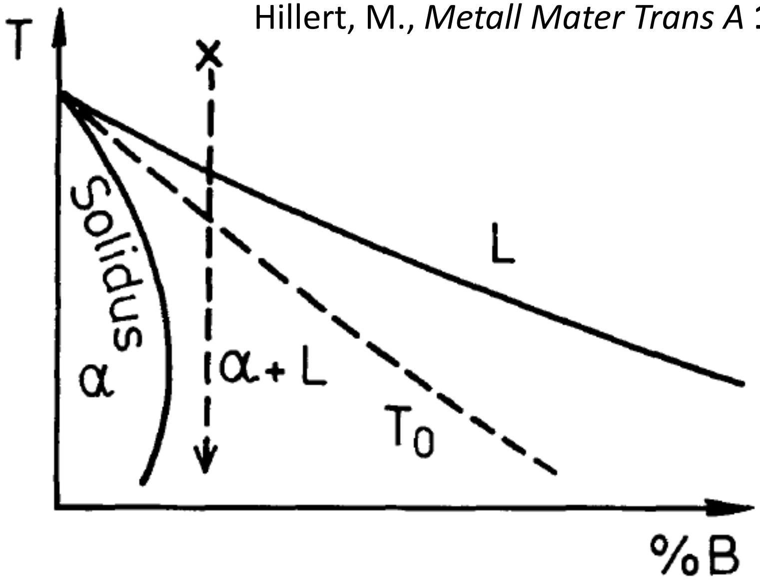

IV. SUMMARY AND CONCLUSIONS

The kinetics of austenitization in mixed ferrite/eutectoid steel have been studied through the use of confocal scanning laser microscopy, dilatometry, and electron microscopy. The following conclusions can be drawn from the combination of results of these experimental methods.

1. Austenite front migration in the ferrite regions of a mixed microstructure, ferrite/eutectoid steel appears to be controlled by long-range diffusion of carbon at temperatures below T_0, and by an interface reaction, proceeding through a massivelike mechanism, at temperatures above. This has been confirmed in both nonisothermal and isothermal experiments.
2. Nonisothermal experiments are consistent with an

Schmidt, E.D. et al., *Metall Mater Trans A* **38**, 698–715 (2007)

T_0 marks the onset of massive formation of austenite.

Austenite formation

Rapid heating conditions

Growth of austenite into ferrite **0,2 %C**

$(Fe,C)^{\alpha} + Fe_3C \rightarrow (Fe,C)^{\gamma}$

$\Delta G^{\alpha+\theta \rightarrow \gamma} = G^{\gamma} - (G^{\alpha})$

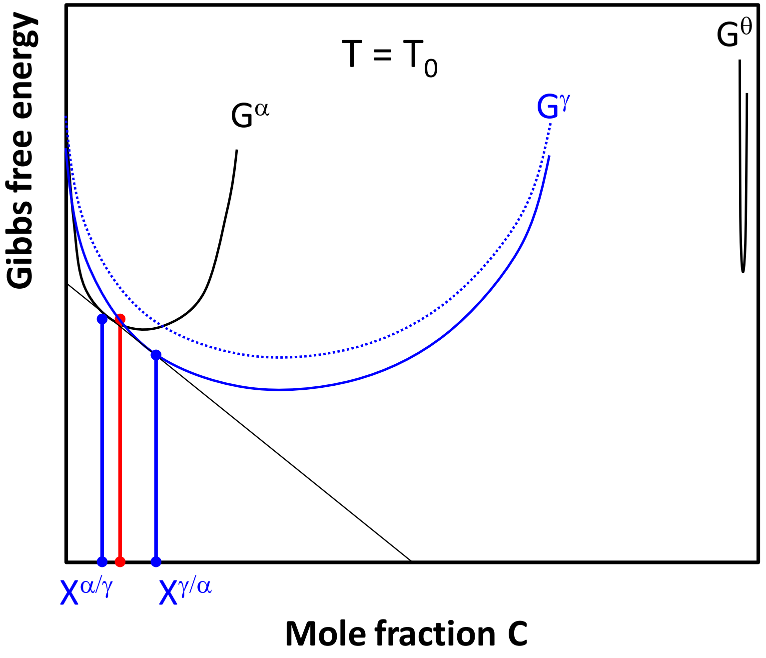

Local Equilibrium is quickly established at high temperatures

Austenite growth is controlled by carbon diffusion

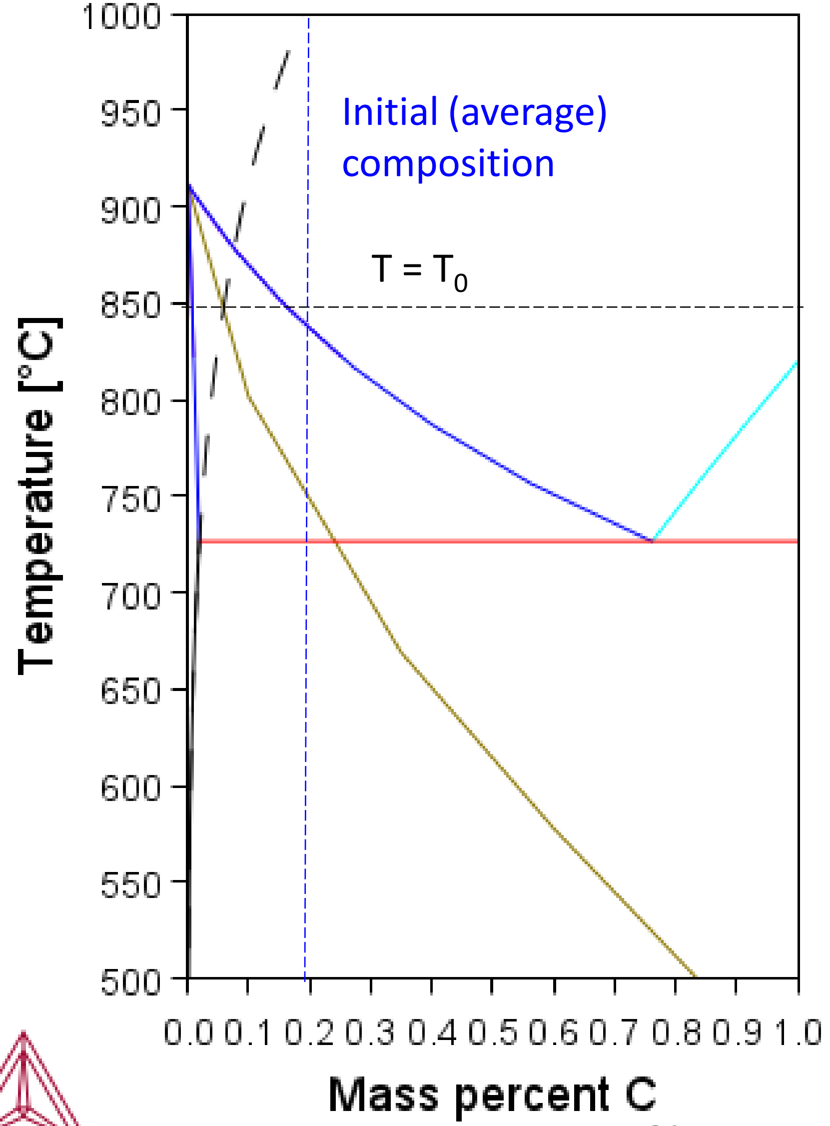

Austenite formation

Rapid heating conditions

Growth of austenite into ferrite 0,2 %C

$(Fe,C)^{\alpha} + Fe_3C \rightarrow (Fe,C)^{\gamma}$

$G^{\alpha} > G^{\gamma}$

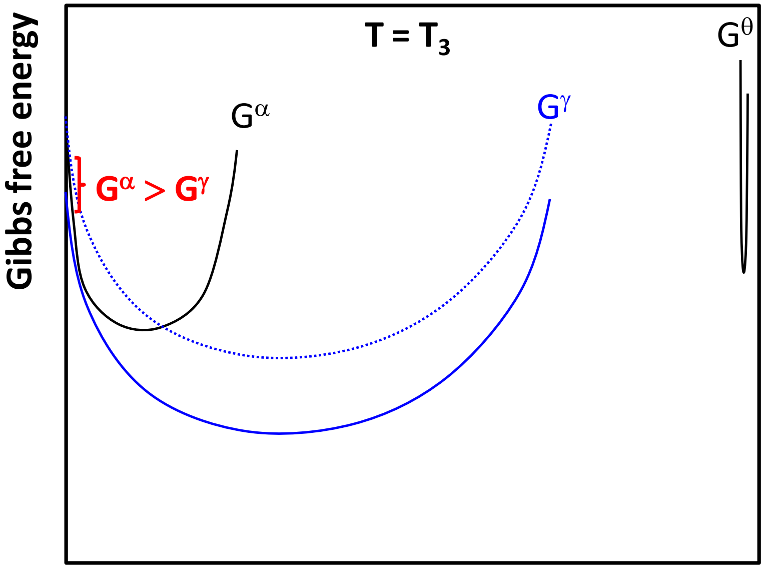

T_P = 898 °C

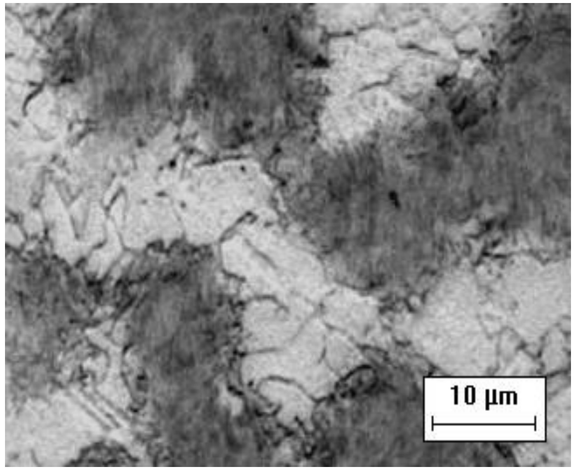

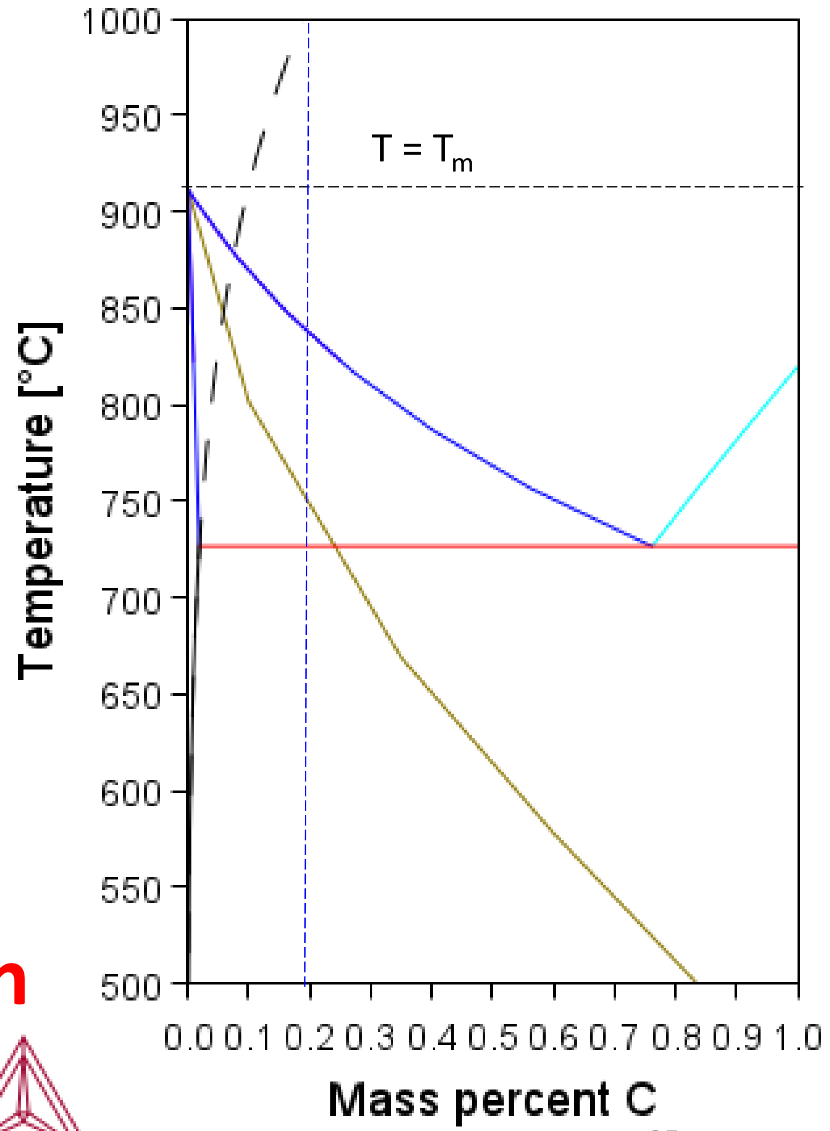

Transition from carbon control to massive

Austenite formation

Rapid heating conditions

Growth of austenite into ferrite **0,2 %C**

$(Fe,C)^{\alpha} + Fe_3C \rightarrow (Fe,C)^{\gamma}$

$G^{\alpha} > G^{\gamma}$

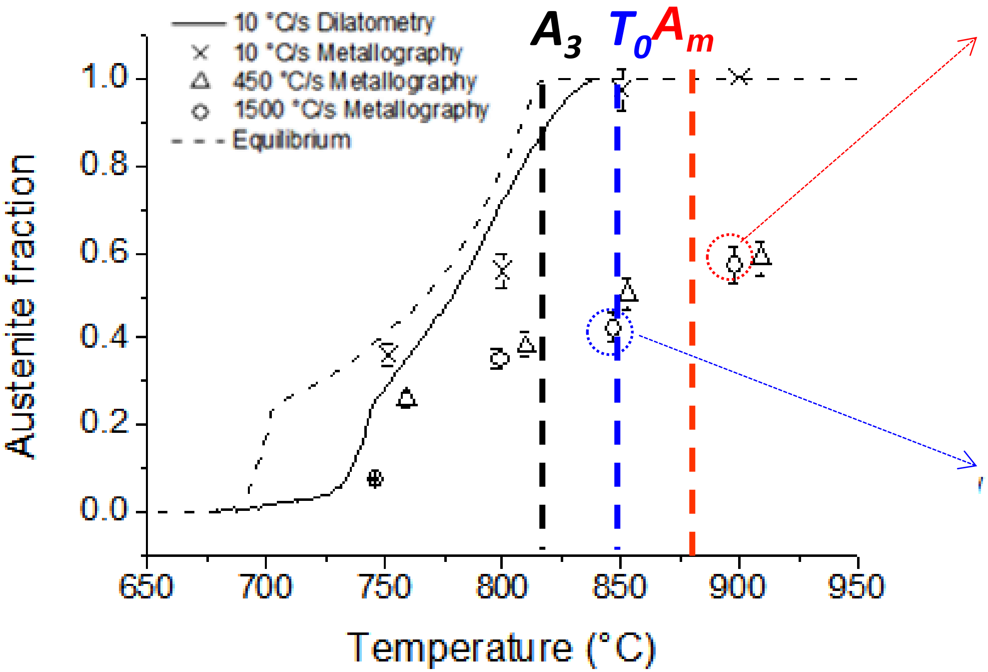

F.M. Castro Cerda et al. Mater. Des. 116 (2017) 448–460

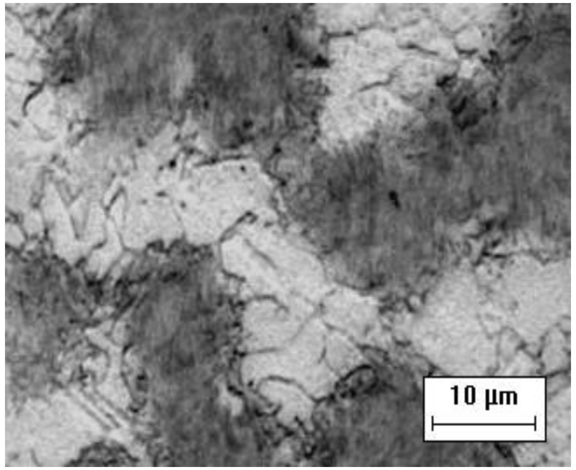

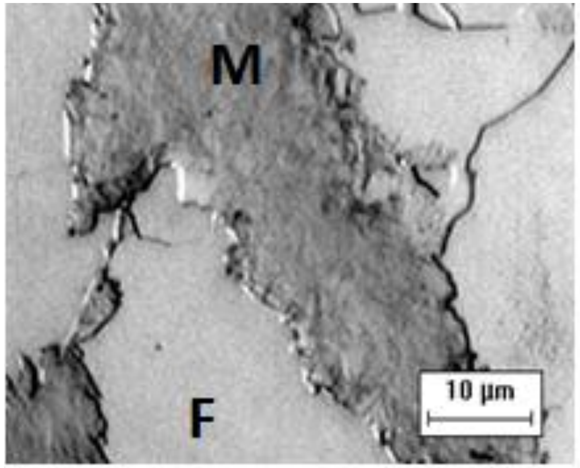

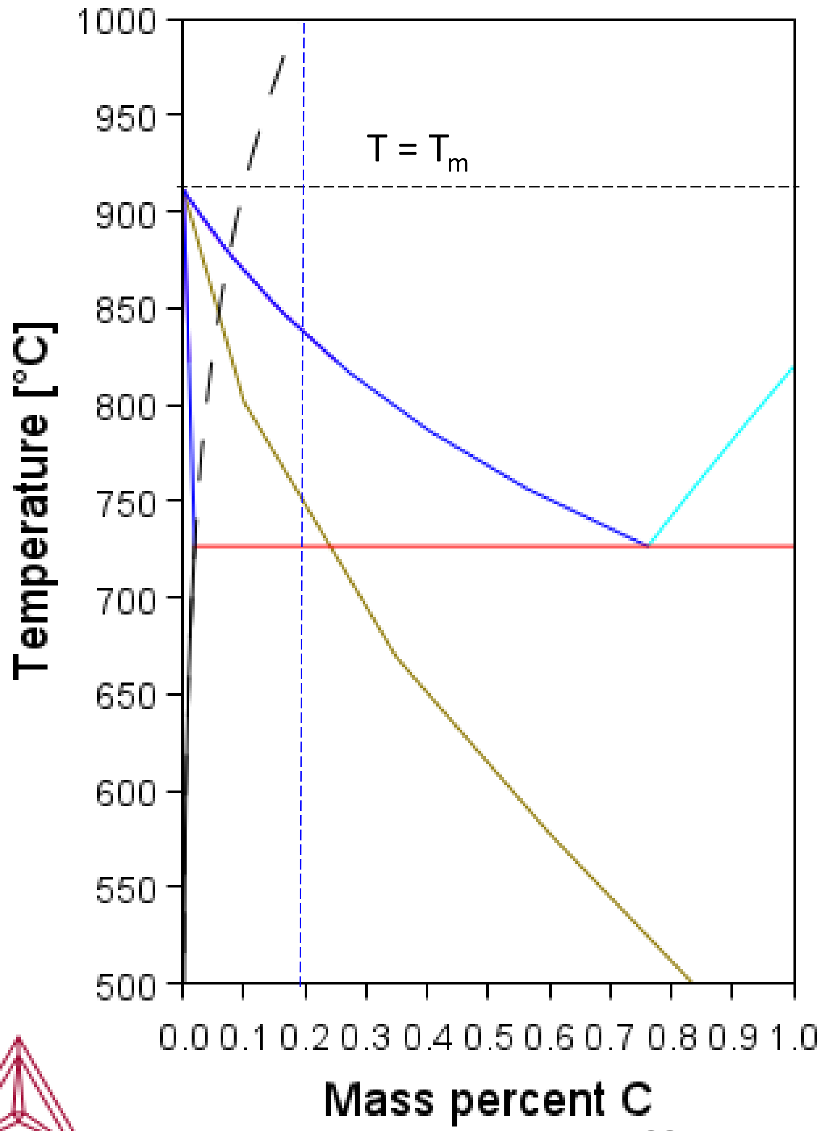

Austenite formation

Rapid heating conditions

Growth of austenite into ferrite **0,2 %C**

$(Fe,C)^{\alpha} + Fe_3C \rightarrow (Fe,C)^{\gamma}$

$G^{\alpha} > G^{\gamma}$

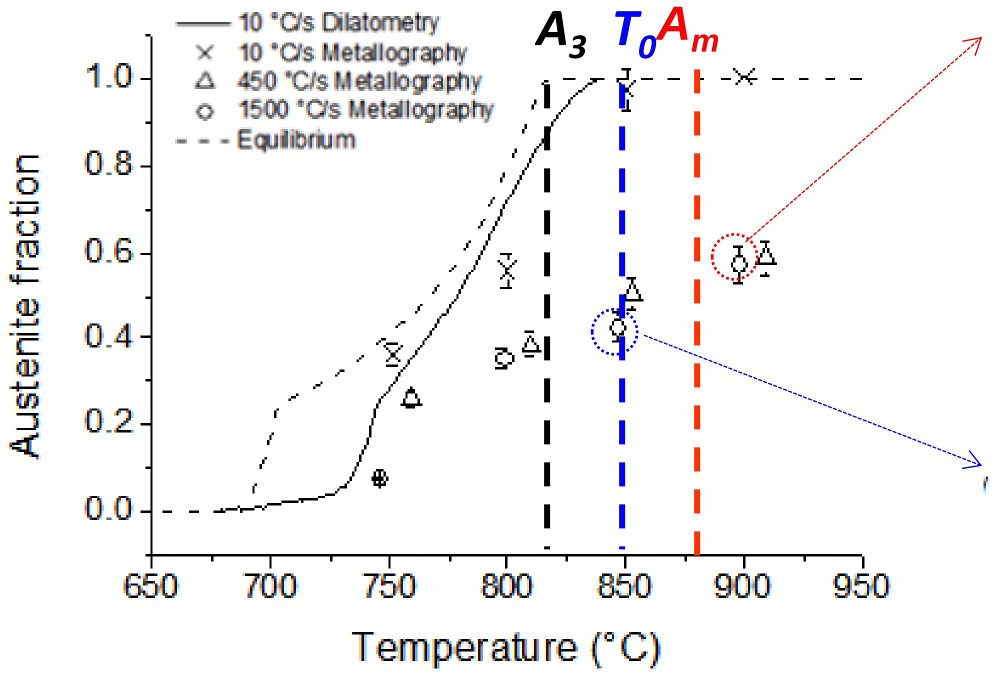

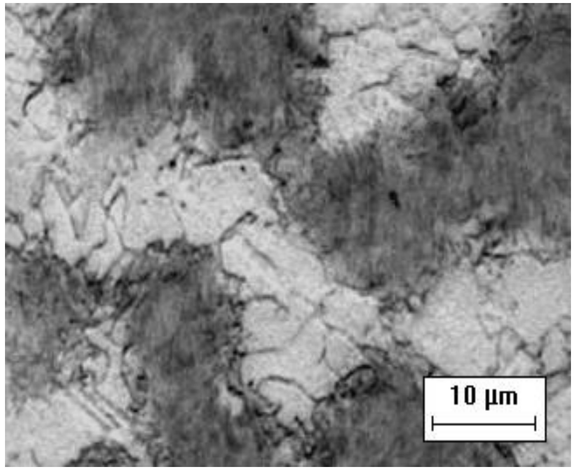

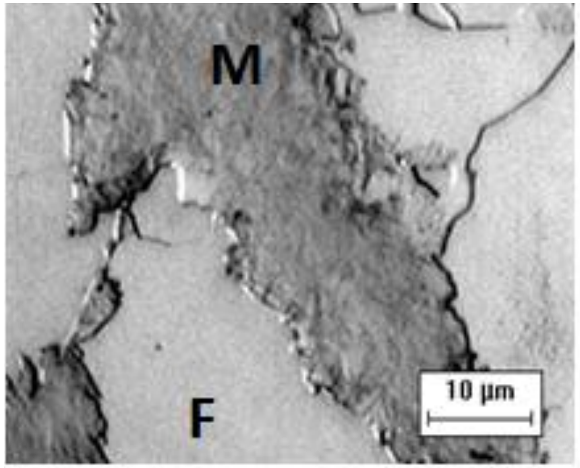

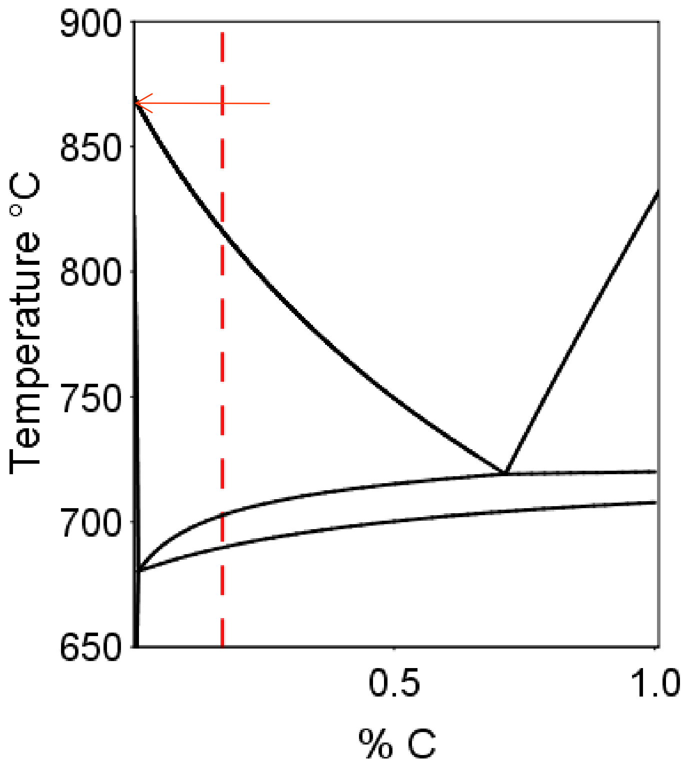

F.M. Castro Cerda et al. Mater. Des. 116 (2017) 448–460

Austenite formation

Rapid heating conditions

Other proposed mechanisms

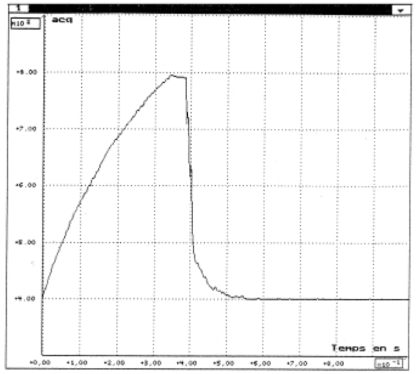

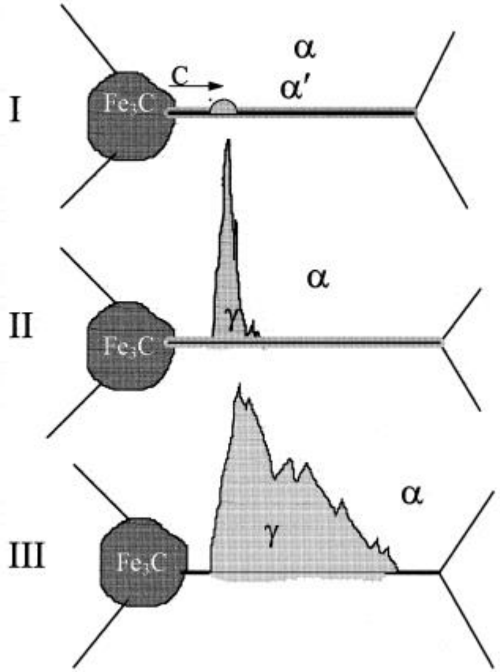

Heating rates of

400 – 1200 °C/s

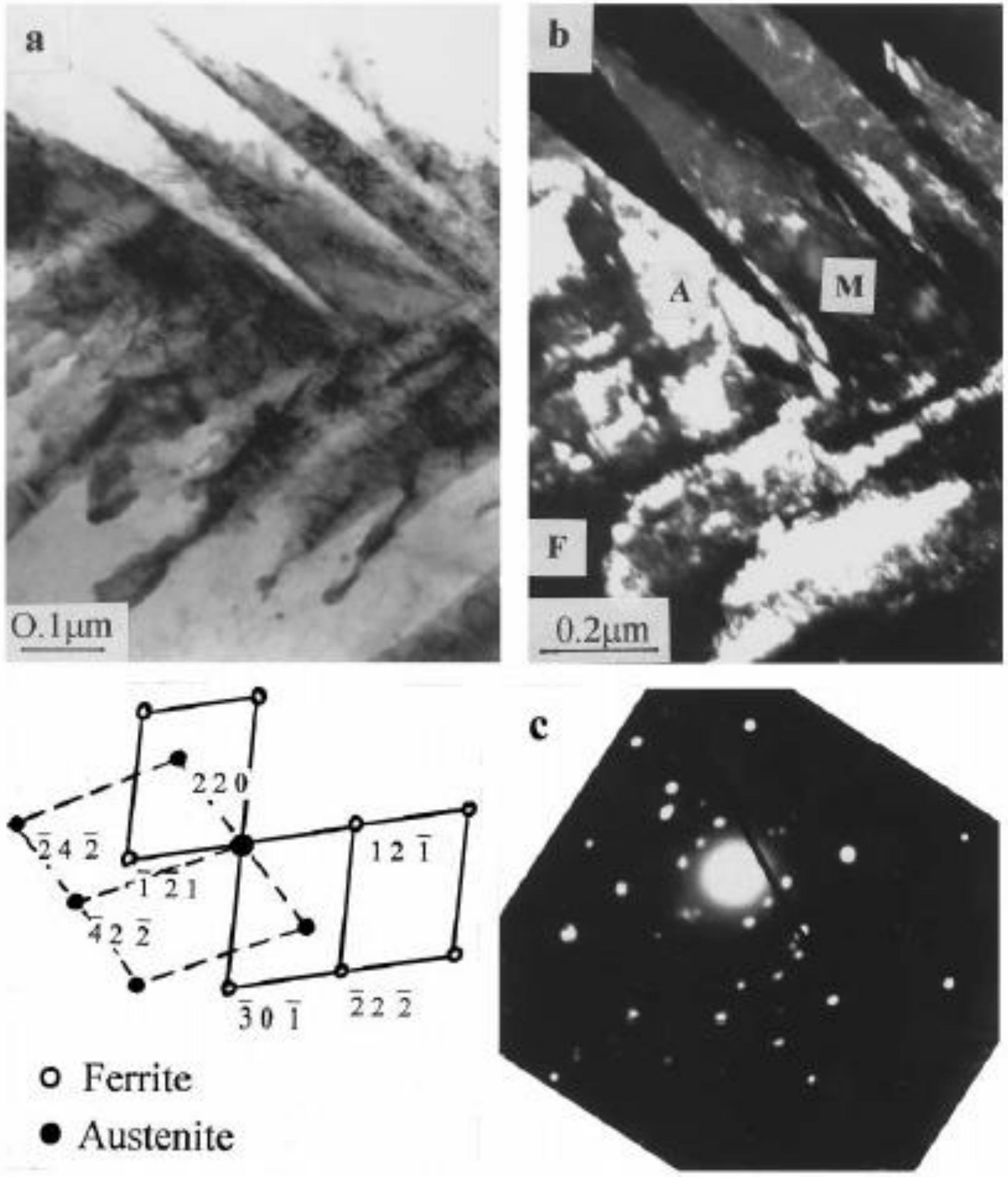

W.J. Kaluba, R. Taillard, J. Foct, The bainitic mechanismof austenite formation during rapid heating, Acta Mater. 46 (1998) 5917–5927.

Quenching and partitioning

Quenched & partitioned steels Aimed to combine martensite and stable austenite

Fe-0.2C-1.9Mn-1.4Si

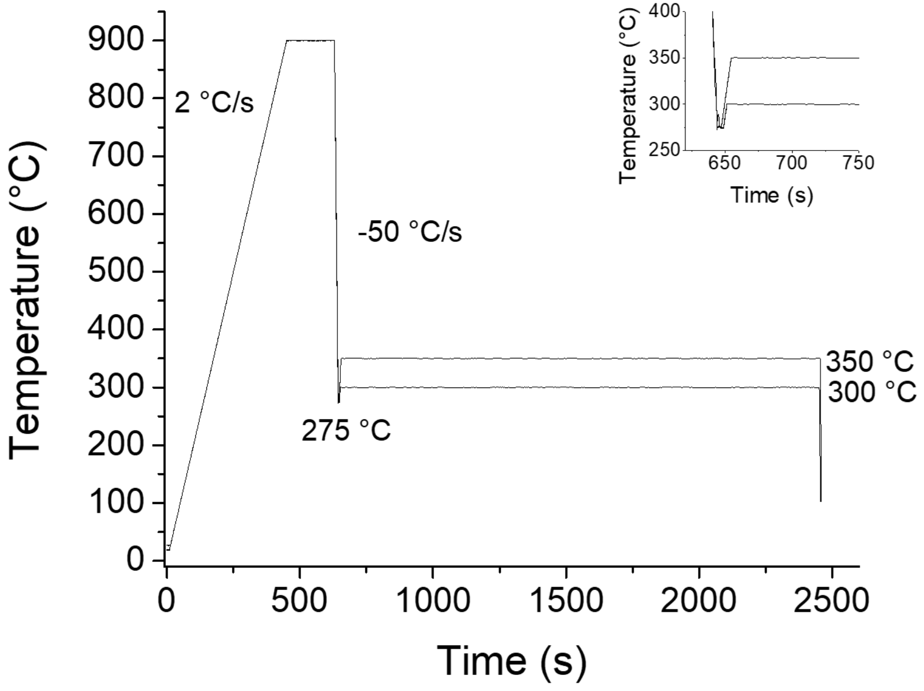

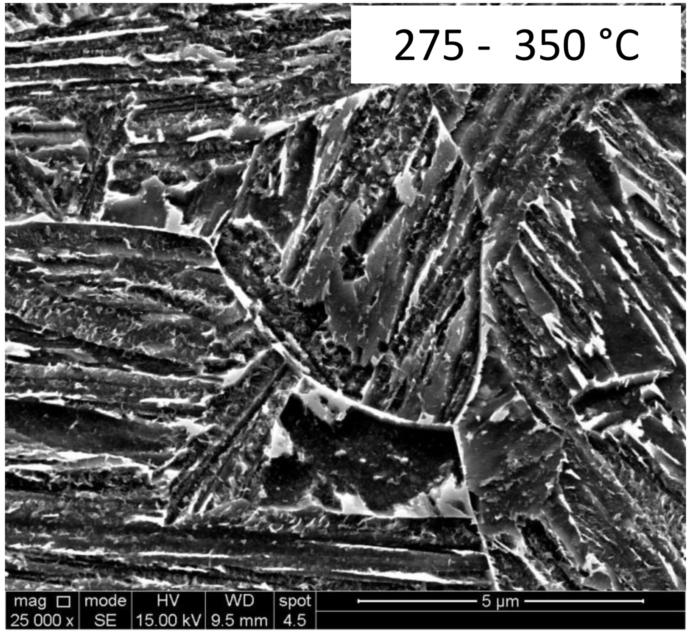

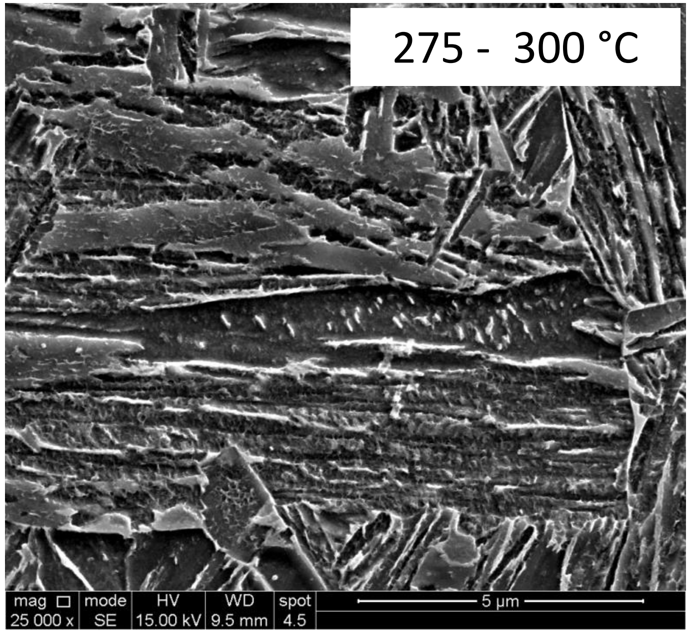

The microstructure is much more complex than we initially predict

FM Castro Cerda et al., Metall Mater Trans A 51, 1506–1518 (2020).

Quenching and partitioning

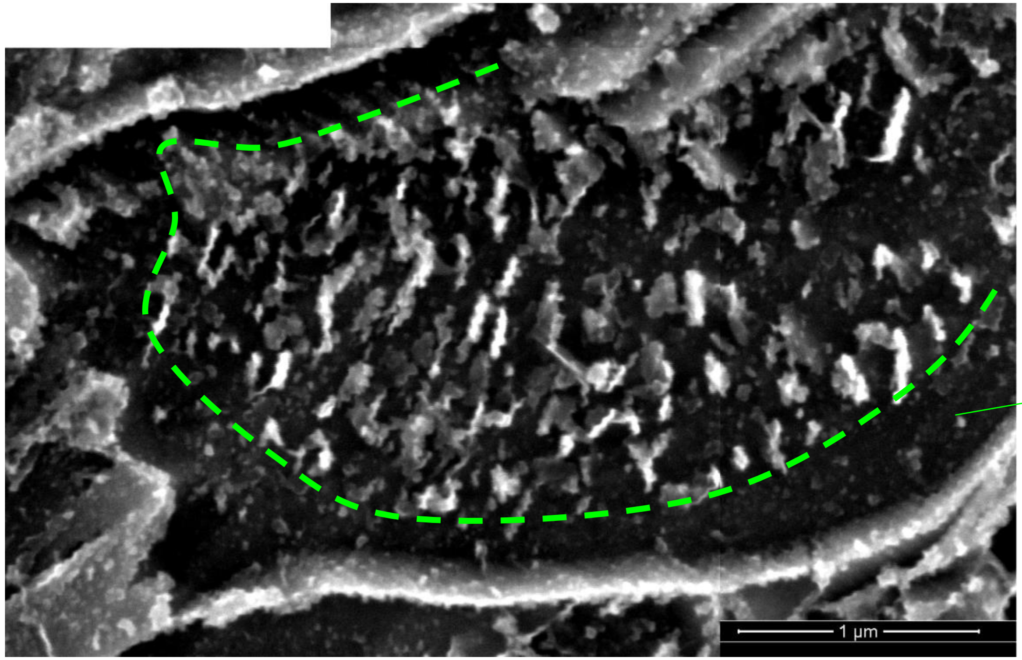

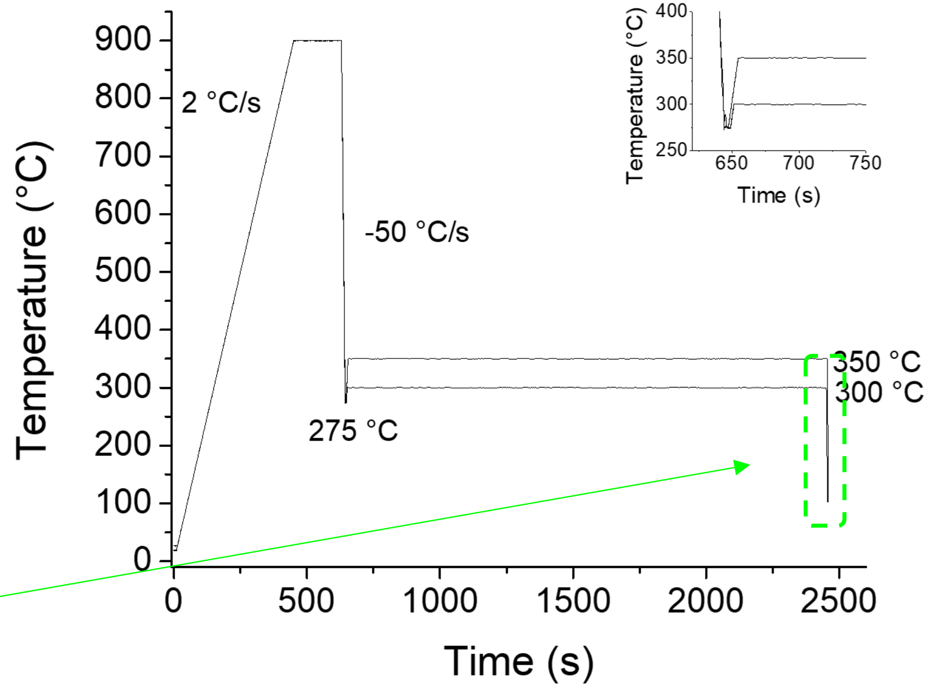

Bainite, as quenched and tempered martensite are also observed

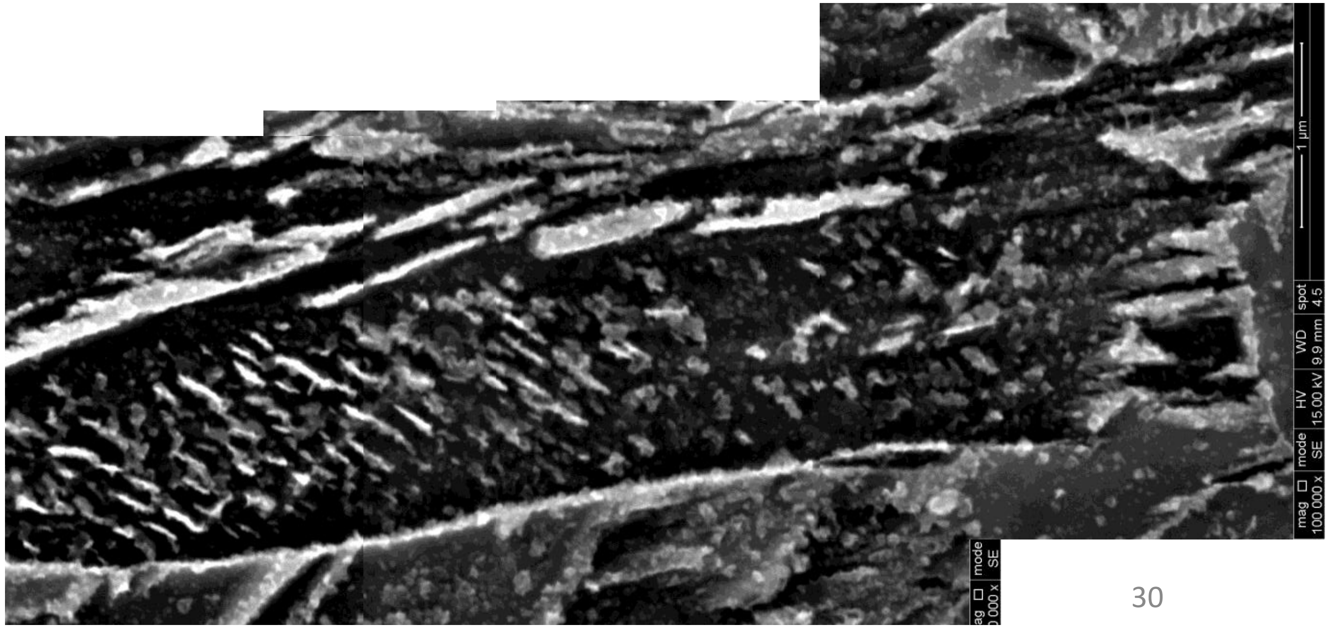

FM Castro Cerda et al., Metall Mater Trans A 51, 1506–1518 (2020).

Constrained carbon equilibrium

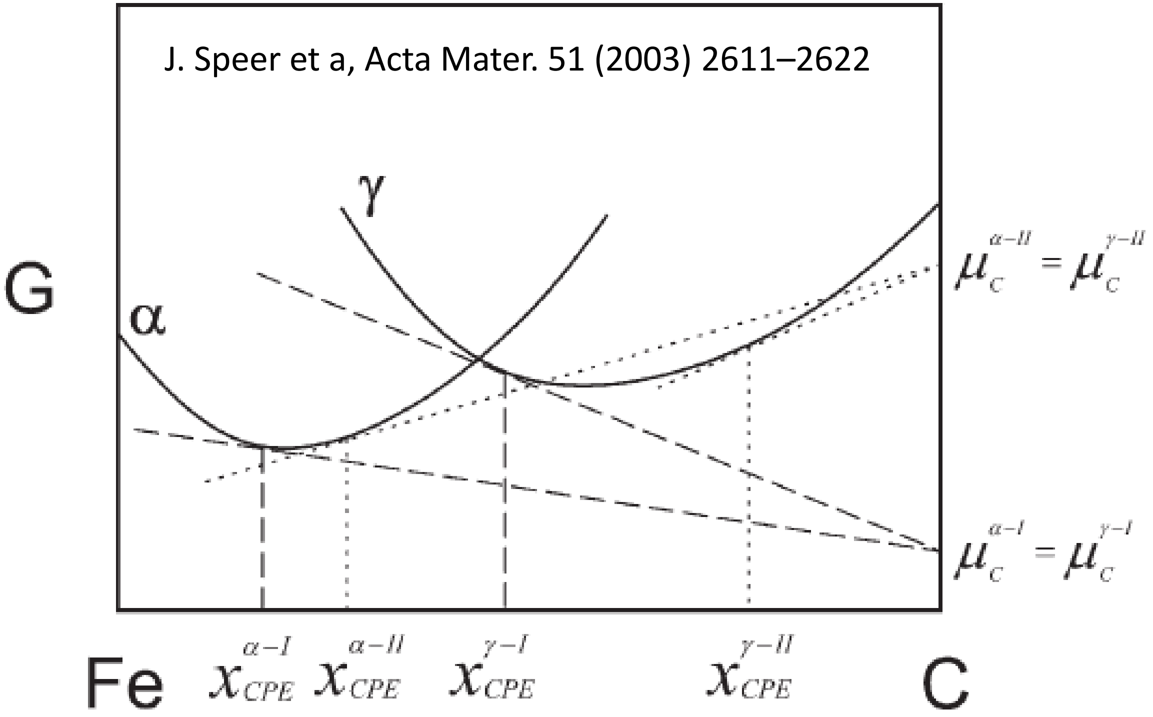

$$f_{CPE}^{\alpha} X_{C_{CPE}}^{\alpha} + f_{CPE}^{\gamma} X_{C_{CPE}}^{\gamma} = X_C^{alloy}$$

Constrained equilibrium between martensite and austenite

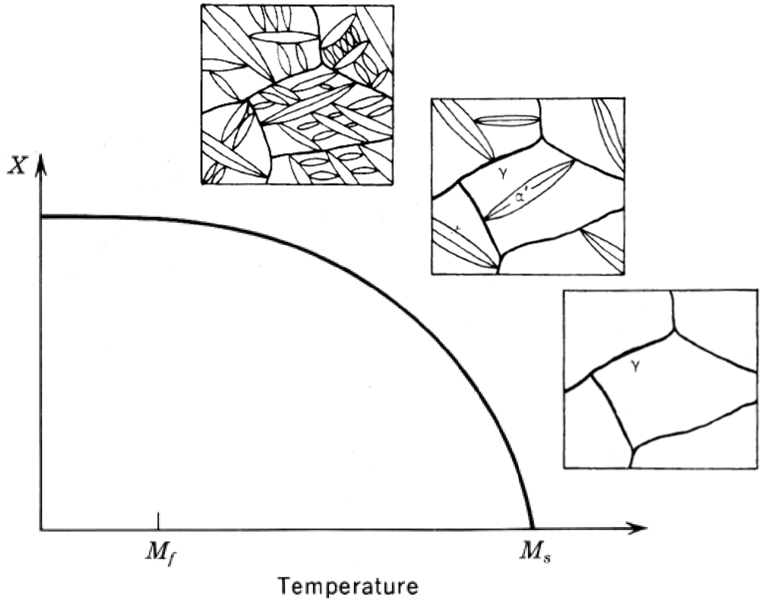

The carbon content of austenite is determined with the mass balance

Constrained carbon equilibrium – Cementite

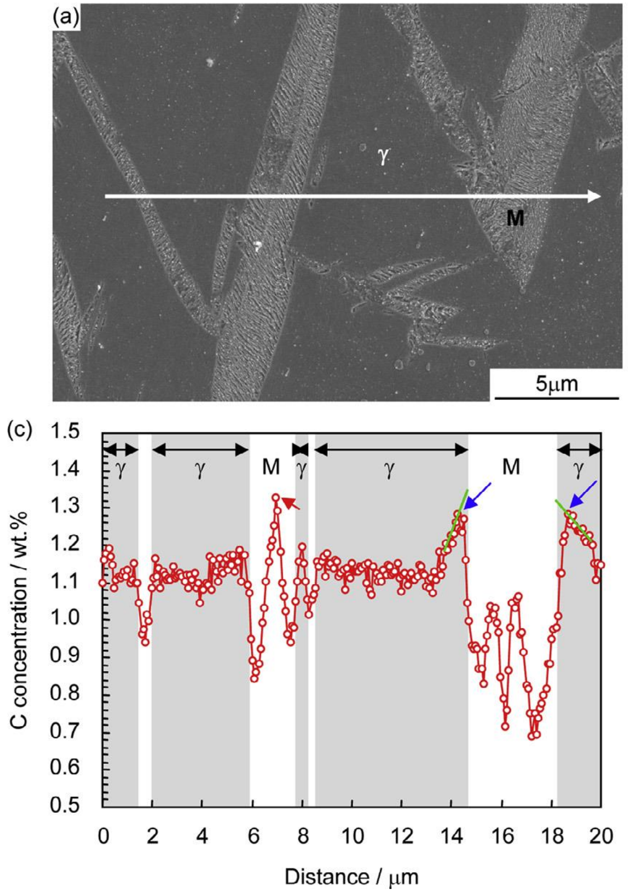

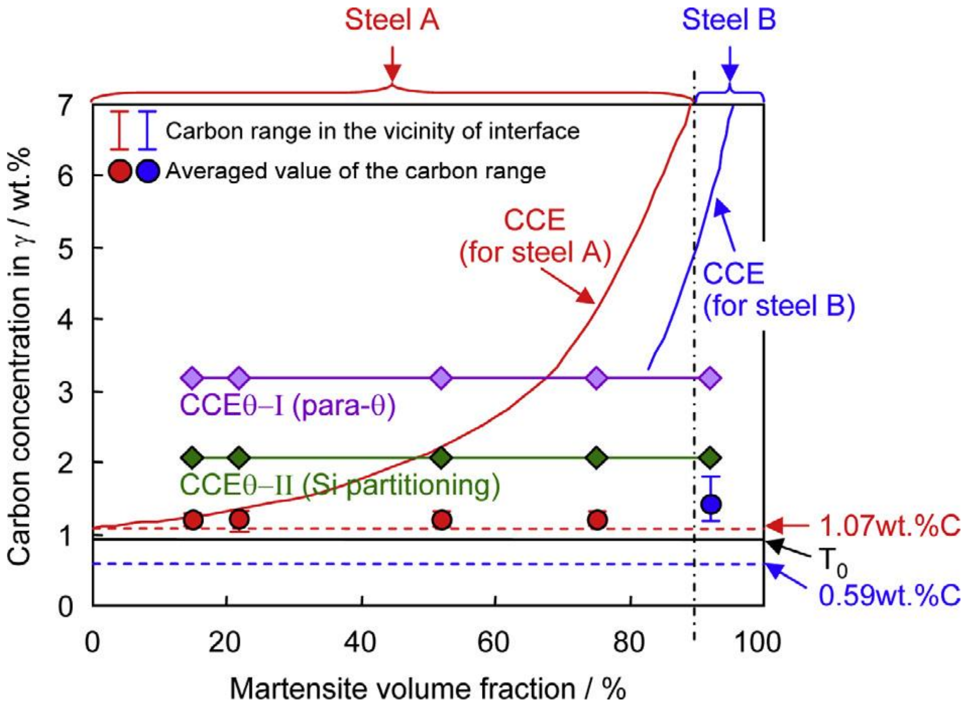

$$\mu_C^\alpha = \mu_C^\theta = \mu_C^\gamma$$

Y. Toji, G. Miyamoto, and D. Raabe: Acta Mater., 2015, vol. 86, pp. 137–47.

The carbon content of austenite is determined by equating the chemical potentials of the three phases

Constrained carbon equilibrium – C balance

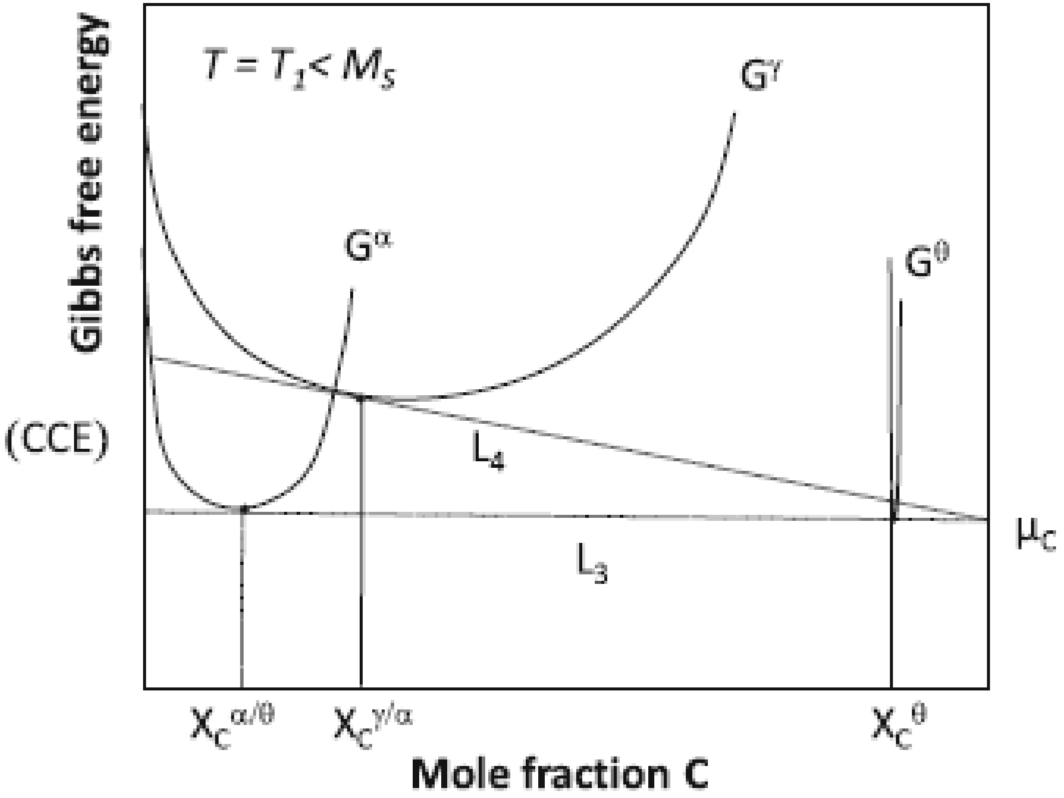

$$X_C^{\alpha'} \times f_V^{\alpha'} + X_C^{\gamma} \times f_V^{\gamma} + X_C^{\theta} \times f_V^{\theta} = X_C^{0}$$

Constrained equilibrium between martensite, austenite and cementite incorporating the mass balance of C

Castro Cerda, F.M., Goulas, C. & Kestens, L.A.I. Metall Mater Trans A 52, 2155–2157 (2021)

Assessment of Q&P steels

Fe-1.07C-2.9Mn-2.2Si

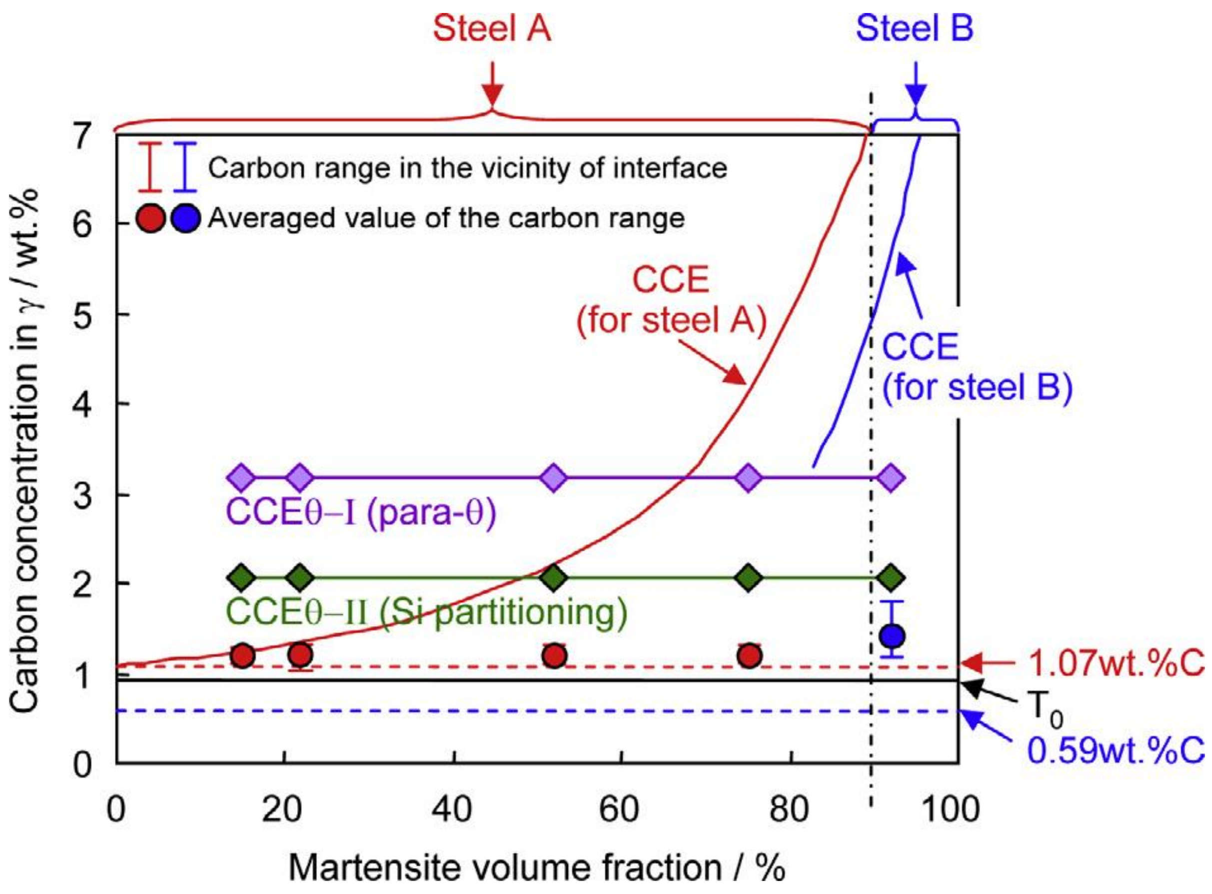

Y. Toji, G. Miyamoto, and D. Raabe: Acta Mater., 2015, vol. 86, pp. 137–47.

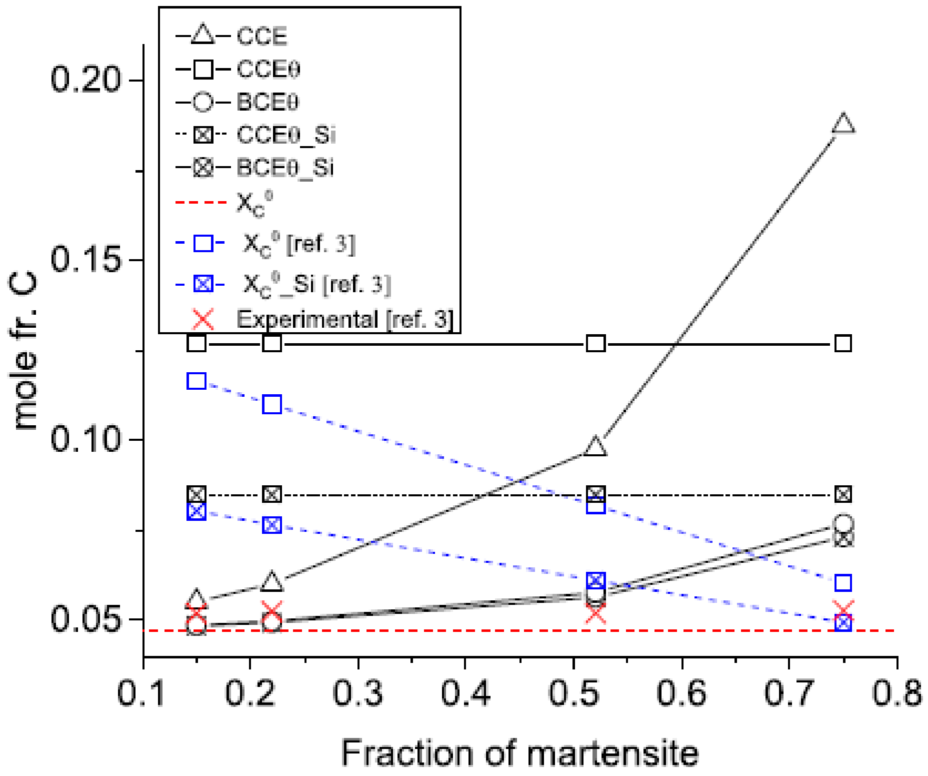

Castro Cerda, F.M., Goulas, C. & Kestens, L.A.I. Metall Mater Trans A 52, 2155–2157 (2021)

CCEθ overestimates the average C content in the alloy

Best fit of BCEθ with experimental data (red crosses)

Assessment of Q&P steels

Fe-1.07C-2.9Mn-2.2Si

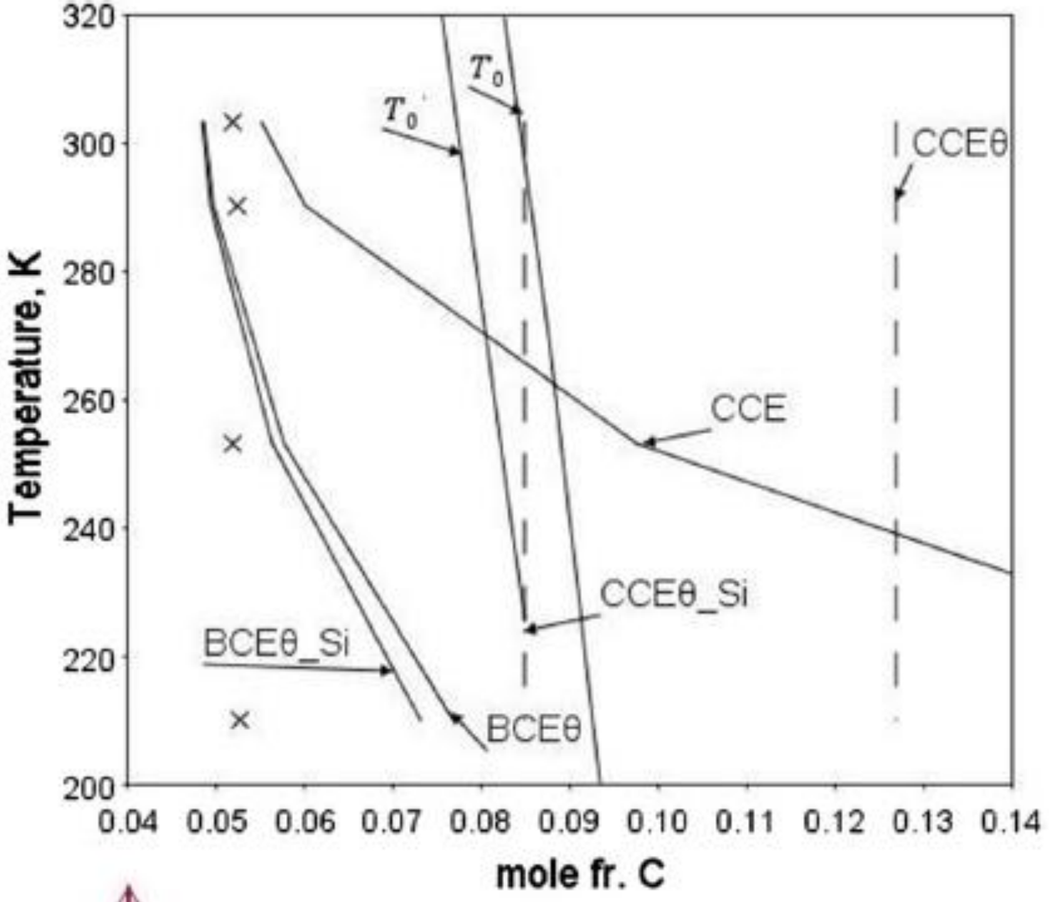

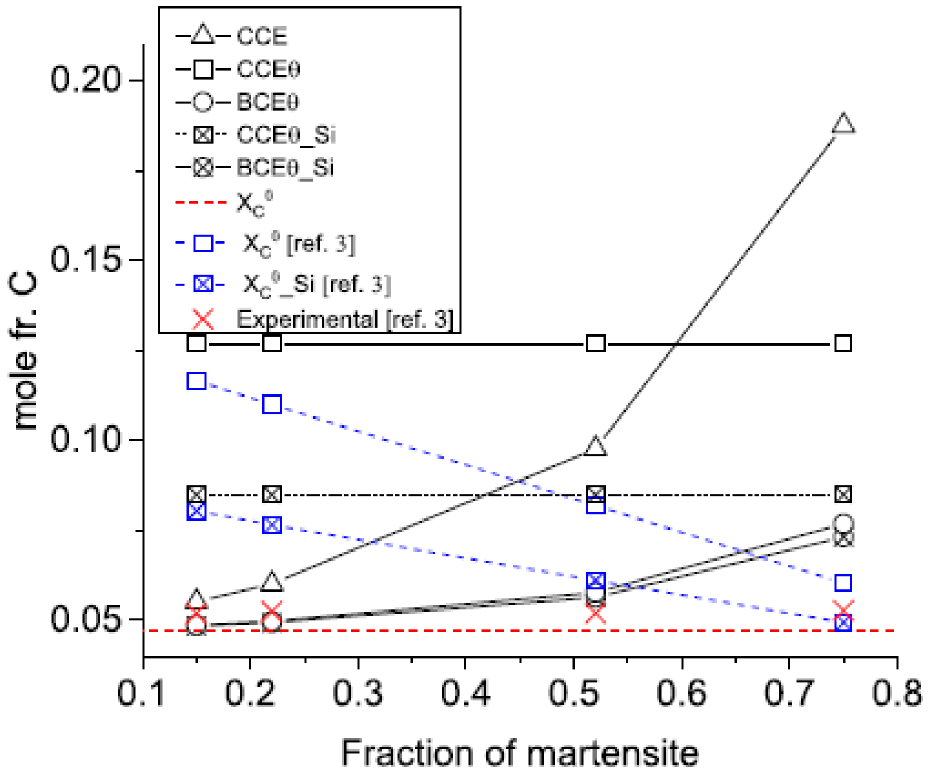

Castro Cerda, F.M., Goulas, C. & Kestens, L.A.I. Metall Mater Trans A 52, 2155–2157 (2021)

CCEθ overestimates the average C content in the alloy

Best fit of BCEθ with experimental data (red crosses)

Assessment of Q&P steels

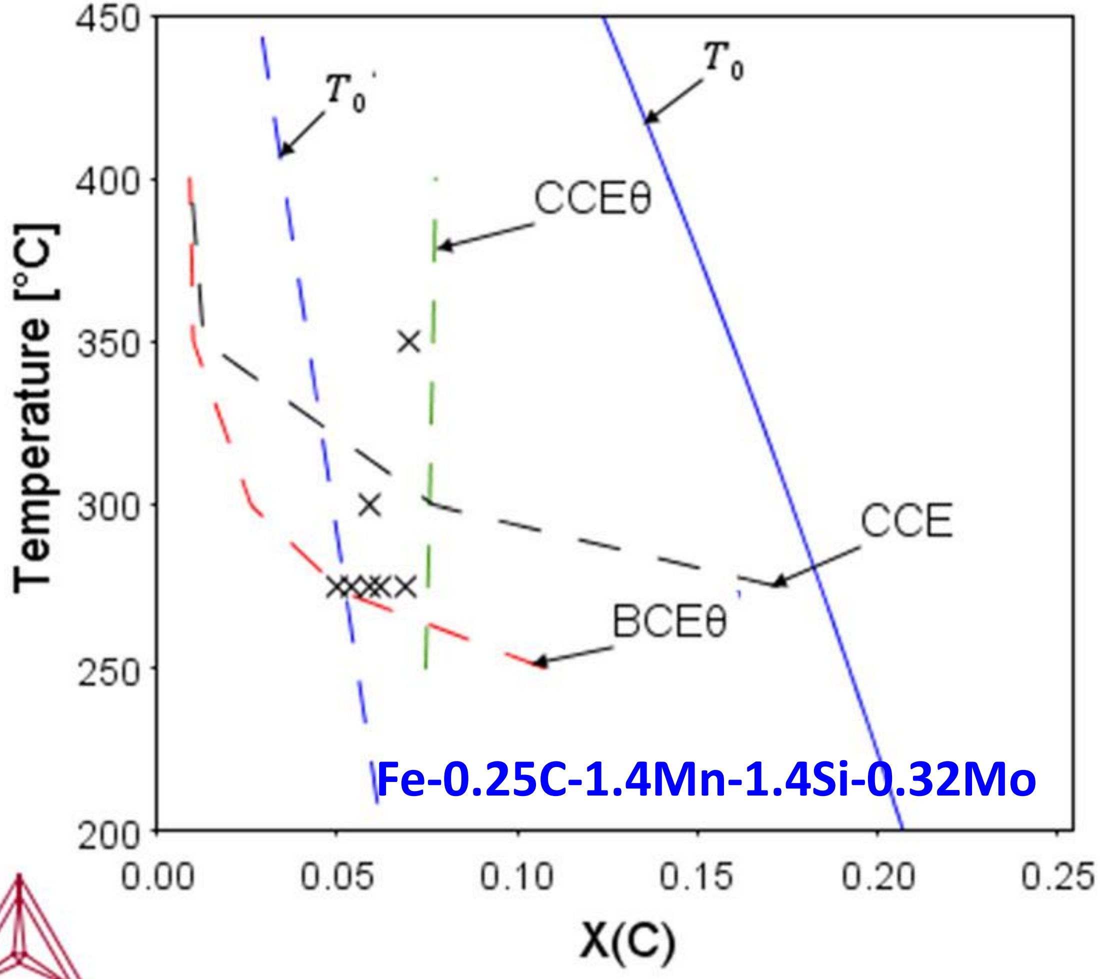

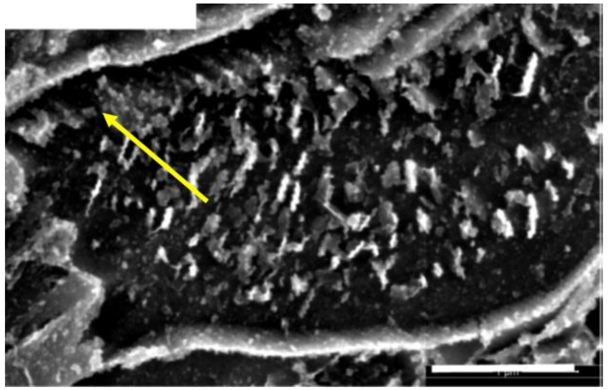

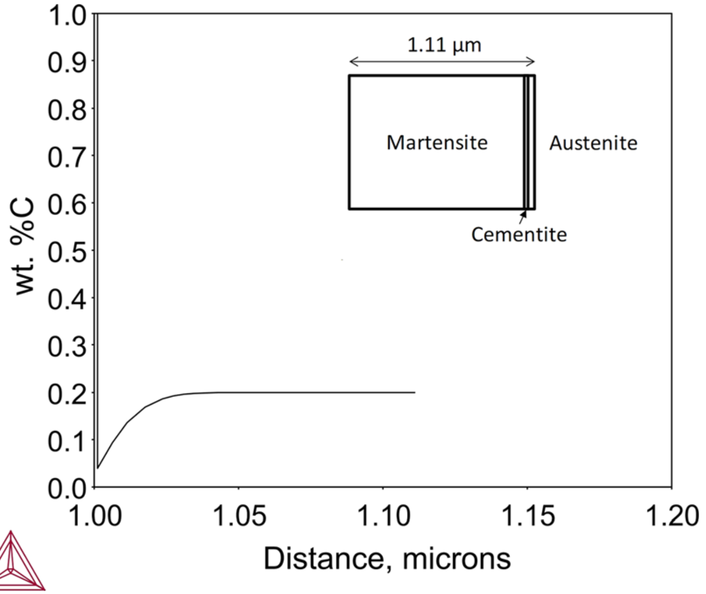

Cementite in contact with martensite on one side and austenite on the other shows that carbon is depleted from austenite after 300 s at 275 °C

The CCEθ model displays the best fit to the experimental data at temperatures near the M_S

FM Castro Cerda et al., Metall Mater Trans A 51, 1506–1518 (2020).

Assessment of Q&P steels

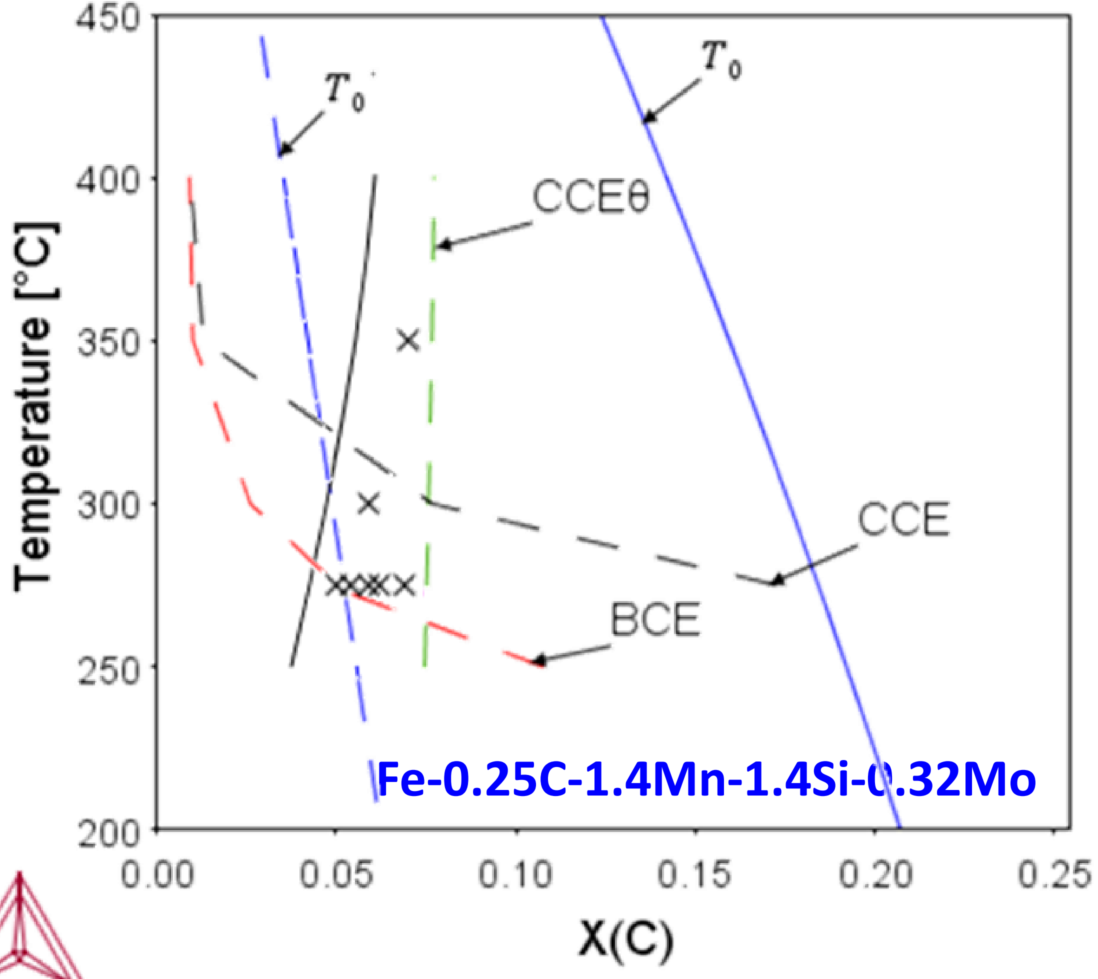

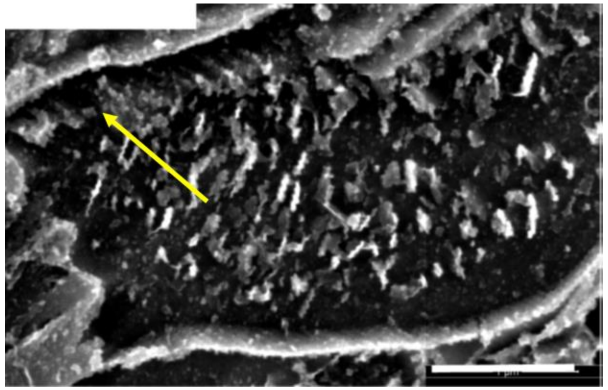

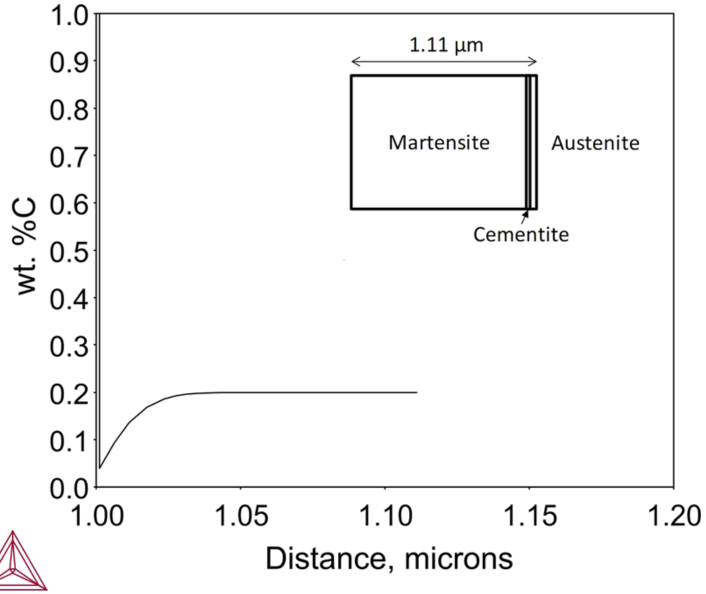

Cementite in contact with martensite on one side and austenite on the other shows that carbon is depleted from austenite after 300 s at 275 °C

WB_S limit composition shows somewhat close relation to the carbon content of austenite

FM Castro Cerda et al., Metall Mater Trans A 51, 1506–1518 (2020).

Assessment of Q&P steels

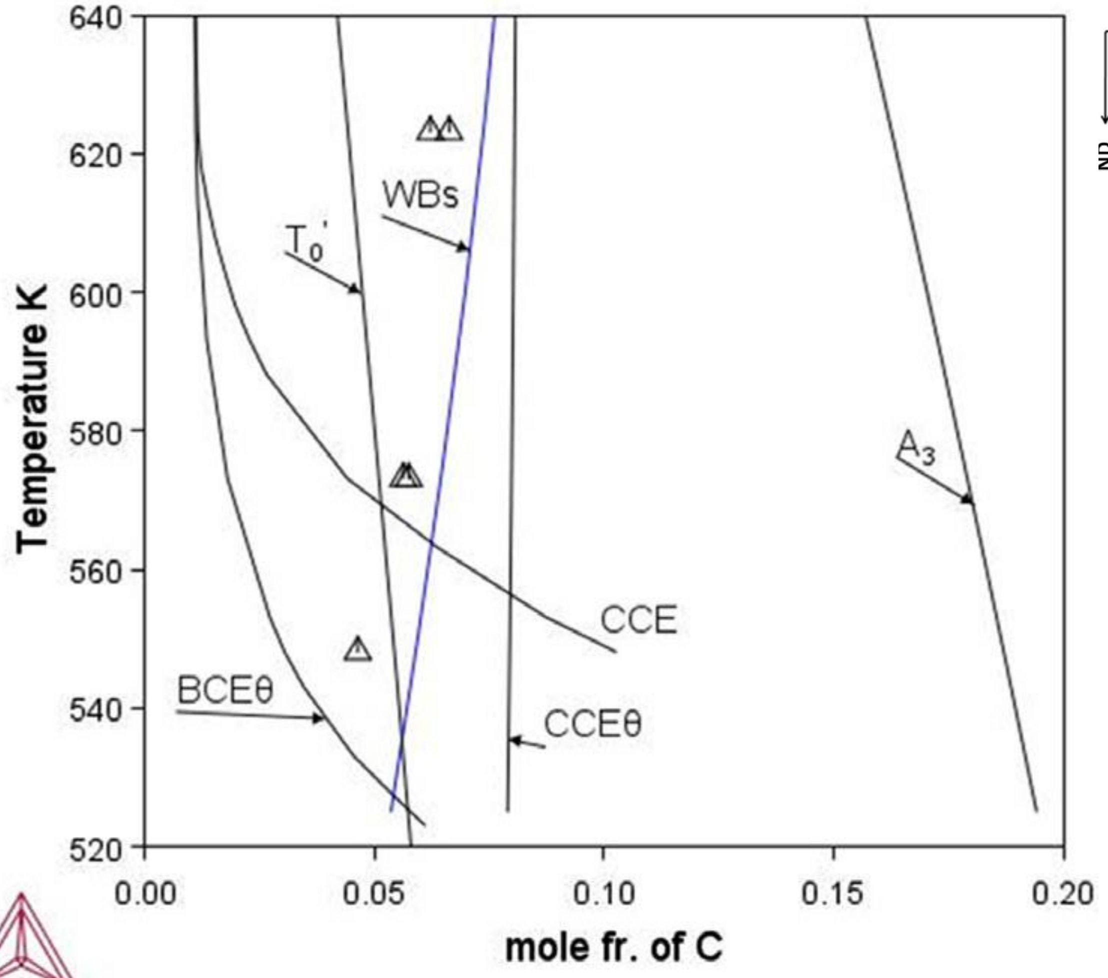

Fe-0.25C-1.4Mn-1.4Si-0.32Mo

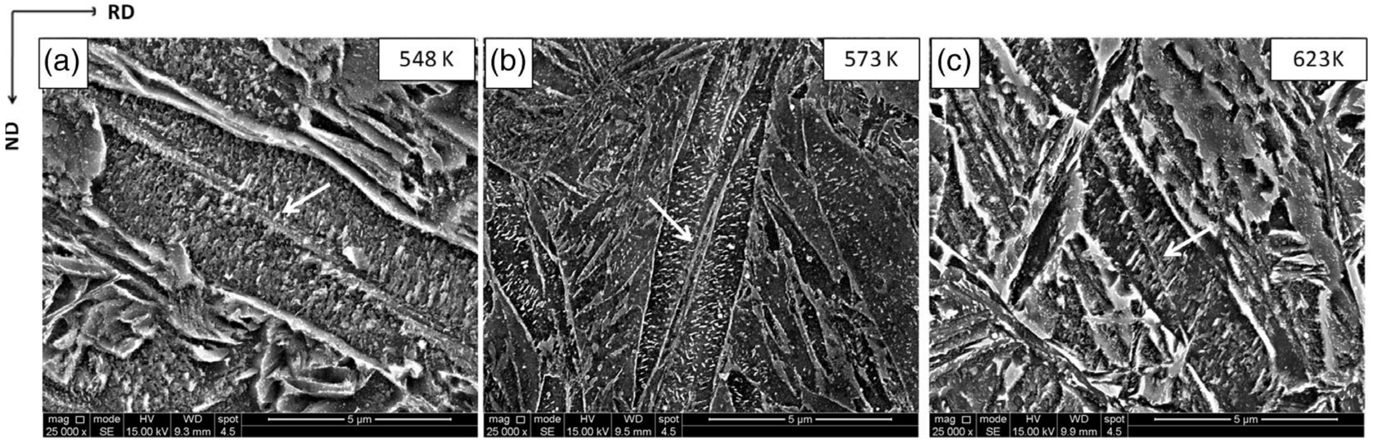

Bainite seems to significantly impact the carbon content of austenite near the M_S

Plate martensite is observed in the microstructure

FM Castro Cerda et al., steel research int. 2023, 94, 2200841

Summary

- ✓ New processing routes may still offer opportunities for further enhancing steel grades
- ✓ Computational thermodynamics is a tool to assist the design new steels chemistries

Aplicaciones de Thermo-Calc y Dictra al diseño de aceros avanzados

Conexiones Thermo-Calc: Aplicaciones y Tutoriales

USACH

Felipe Castro Cerda
Associate Professor
Dept. of Metallurgy

Martes 15 de Octubre 2024